Regional and Seasonal Variations of Surface Reflectance from Satellite Observations at 0.6 μm

ELAINE MATTHEWS* AND WILLIAM B. ROSSOW

NASA Goddard Space Flight Center, Institute for Space Studies, New York, NY 10025

(Manuscript received 17 March 1986, in final form 25 July 1986)

ABSTRACT

A global series of seasonal visible surface reflectance maps derived from NOAA-5 Scanning Radiometer observations is presented. Methods for isolating clear-sky observations from satellite data are evaluated and the magnitude of atmospheric effects (Rayleigh scattering and ozone absorption) are presented. A preliminary analysis of digital vegetation and soils data bases, which were analyzed in conjunction with the satellite observations, is discussed. Regional and global reflectance homogeneity of land-cover types, and snow brightening for types, are presented. Results demonstrate that the statistical approach for isolating clear-sky radiances used in this study obtains accurate enough values for each location to allow meaningful measurements of seasonal, spatial and ecosystem variations in surface reflectance.

1. Introduction

Since the earth's atmosphere is relatively transparent to solar radiation, surface albedo and cloud albedo are key determinants of the planetary, atmospheric and surface energy budgets. The success of attempts to model the climate is consequently dependent, in part, on the accuaracy of modeling the solar radiation reflected and absorbed at the surface. The variability of radiation reflected from land surfaces is governed primarily by variations in vegetation type, structure, coverage and condition, although arid areas vary due to differences in soil and rock properties. The dominant role of vegetation provides a possible feedback on climate changes, especially through the effect of vegetation on snow brightening of surfaces.

The heterogeneity of vegetation types and coverage makes accurate specification of global surface albedo difficult; however, high-resolution satellite observations provide a means, in principle, to study the radiative characteristics of different surface types and to survey the global distribution of surface albedo. Further, these observations can be used to characterize the brightening, caused by snow cover, of each vegetation type or location. Such results will not only improve the specification of surface albedo in simulations of the current climate, including long-range weather forecasts, but allow for better prediction of changes in surface albedo with changes in vegetation induced by climate variations. Additionally, improved modeling of surface reflectances can improve the sensitivity of satellite monitoring of vegetation changes, which may be indicative of regional or global climate variations or man-made changes.

The present analysis of NOAA-5 Scanning Radiometer measurements of visible (~0.6 μm) radiances is an exploratory study of the utility of current satellite observations for the study of surface albedo and its variations in space and time. This study focuses on evaluation of methods for isolating clear-sky observations from satellite images and assesses the importance of some corrections for atmospheric effects on the measured radiances. As part of these tasks, we also provide preliminary assessments of a global vegetation cover-type classification (Matthews, 1983, 1985), of the regional and global homogeneity of each land-cover type, and of variations of snow brightening for each type. Although we do include the dependence of surface reflectance on solar zenith angle in studying the seasonal variation of surface reflectances, this study does not consider either the full angular dependence or spectral dependence of radiation reflected from the surface; hence, the maps presented are of surface *spectral reflectance,* not albedo.

Data used for this exploratory study are one year's global observations from the NOAA-5 Scanning Radiometer (SR), which measures visible radiance (0.52–0.72 μm) and infrared radiance (10.5–12.5 μm) (Fig. 1). Observations are made once per day in the morning over the whole globe. The radiometer field-of-view resolution is 4 and 8 km at nadir for visible and infrared, respectively, but the data are sampled to provide one observation per 15–25 km. Since the precise location of the observation is unknown over this same scale, the surface resolution is statistically equivalent to ~20 km.

* MA Com Sigma Data, New York, NY 10025.

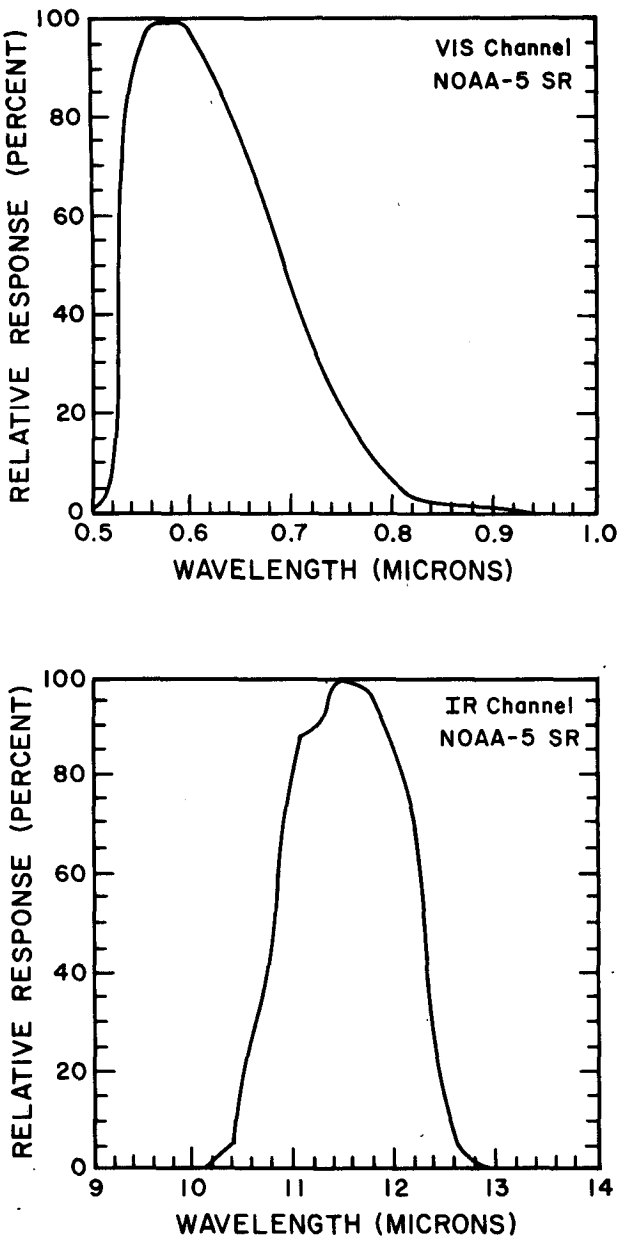

FIG. 1. Spectral response of NOAA-5 Scanning Radiometer channel 1 (visible) and channel 2 (thermal infrared).

The visible channel on the NOAA-5 SR appears to have a noise level of about 2% rms (Rossow et al., 1987). Since most surfaces have reflectivities between 5–15%, this noise is equivalent to about 15–40% (relative amplitude) noise for a single measurement. If some averaging of reflectances is performed, the uncertainty at 5% can be reduced to <2% in absolute reflectance. (This is a formal error estimate only; we assess the noise level in this study.) Absolute calibration of these data may only be accurate within 10–15%, but comparisons of the results to independent data suggest an absolute uncertainty of ~3% near zero and ~10% at high reflectance (Rossow et al., 1987).

Section 2 briefly reviews previous studies of surface albedo to assess the current understanding of this problem. Section 3 considers the magnitude and importance of atmospheric effects on satellite-measured radiances that must be removed to obtain measurements of surface properties. The most important atmospheric effect is produced by clouds; section 4 discusses methods used to isolate clear-sky observations in the data. In section 5 we present the results of an analysis of 5 months of NOAA-5 Scanning Radiometer data (January, February, April, July and October 1977) covering the whole globe, to determine what information about spatial and temporal variations can be extracted from this type of data. Section 6 summarizes the measurement uncertainties and information content of visible band data and outlines the next steps in improving our knowledge of global surface albedo.

2. Previous work

The numerous studies related to surface reflectivity or albedo that have been conducted vary in spectral coverage, seasonal and spatial coverage, instrument platforms, cloud-removal and atmospheric-correction methods, and purpose.

a. Surface and aircraft observations

Many workers have carried out studies of spectrally integrated albedo in small areas with hand-held radiometers or airborne sensors. These studies are often designed to measure seasonal variations of albedo for specific cover types (see, e.g., Bauer and Dutton, 1962; Stanhill et al., 1966; Chia, 1967; McFadden and Ragotzie, 1967; Oguntoyinbo, 1970; Berglund and Mace, 1972; Petzold and Rencz, 1975; Arnfield, 1975; Monteith, 1975, 1976; Howard, 1977; LeMaster et al., 1980). Kung et al. (1964) carried out a more extensive flight survey, measuring integrated surface albedo from airplane-mounted radiometers over the course of a year. They produced seasonal albedo maps of North America, based on intensive flights over various land-cover types in Wisconsin in conjunction with more sporadic continental flights and continental land-cover data.

There are also many reflectance measurements with more detailed spectral coverage available, but usually the results are for very limited areas or only a few vegetation types, and often for single days or concentrated in the growing season. These studies frequently focus on agricultural crops to investigate seasonal relationships between spectral reflectance and vegetation characteristics such as biomass or yield (see, for e.g., Monteith and Szceicz, 1961; Olson and Good, 1962; Scott et al., 1968; Kanemasu, 1974; Monteith, 1976; Tucker, 1978; Fuller and Rouse, 1979; Tucker et al., 1980;

LeMaster et al., 1980; Richardson and Gausman, 1982; Tucker et al., 1981).

In addition to the studies mentioned above, there is a body of reflectance-measurement data that are usually spectrally discrete for a single date or conducted in a laboratory (see, e.g., Condit, 1970; Hoffman, 1970; Root and Miller, 1971; Leeman et al., 1971; Leeman, 1972; Tucker, 1978; Kriebel, 1979).

These types of measurements have been combined with global land-cover data bases to infer global surface albedo (Posey and Clapp, 1964; Hummel and Reck, 1979; Kukla and Robinson, 1980; Robock, 1980; Briegleb and Ramanathan, 1982) and to improve parameterizations of surface albedo in climate models (Hummel and Reck, 1979; Dickinson, 1983; Matthews, 1984; Wilson, 1984). However, validation of such global representations has been hampered by the lack of consistent, seasonal data sets of spectral reflectance measurements at regional and global scales.

b. *Satellite observations*

1) PLANETARY ALBEDO

Studies of the radiation budget at the top of the atmosphere (TOA) have been made using a variety of satellite measurements (e.g., Vonder Haar and Suomi, 1971; Raschke et al., 1973; Gruber and Winston, 1978; Jacobowitz et al., 1984). One element of this radiation budget is the planetary albedo, which includes the effects of surface, clouds and atmosphere, integrated over all angles and wavelengths. The actual measurements have covered both narrow and broad spectral intervals and sampled only limited portions of the complete reflection geometry; hence, various strategies are used to infer the total planetary albedo. Some of these studies have also isolated clear-sky *planetary* albedos for a few surface types (Minnis and Harrison, 1984; Taylor and Stowe, 1984); but, since the effects of atmospheric scattering and absorption have not been removed, these results are not measures of the surface albedo. Recently, Briegleb et al. (1986) have compared modeled with observed TOA albedos. The observations were broadband albedos derived from narrowband GOES-2 minimum brightness; modeled albedos incorporated prescribed narrowband surface reflectances for vegetation types as well as effects of solar zenith angle, orography, and surface and atmospheric absorption/scattering.

2) SURFACE ALBEDO

Studies aimed at deriving surface reflectance properties from satellite measurements have incorporated several methods of calibrating broad- and narrow-band satellite observations and correcting for atmospheric effects. Rockwood and Cox (1976) correlated the visible (0.55–0.75 μm) SMS-1 system brightness with limited broadband (0.285–2.8 μm) airplane-flight measurements to investigate seasonal variations in Sahelian surface albedo. Mekler and Joseph (1983) proposed a method for deriving spectral surface reflectance from LANDSAT imagery in which three single-band ground measurements in a scene, at reflectance extrema, are used to calibrate the satellite scene. The method is valid for aerosol optical depths of ≤ 0.75 and was tested over low-latitude desert areas, assuming a single aerosol mode and humidity profile. Courel et al. (1984) used a series of temporally overlapping Meteosat-1 and LANDSAT data to reconstruct the albedo history of a Sahel/Sahara region for the period 1972–79: cloudy scenes were excluded by visual examination of images; corrections for Rayleigh scattering, ozone and water vapor absorption, and aerosol scattering were incorporated.

Imagery from the Defense Mapping Satellite Project (DMSP), processed with a densitometer and calibrated with specified surface albedos for certain areas, has been used to produce maps of maximum winter albedo for seasonally snow-covered regions of the Northern Hemisphere (Robinson, 1984). Chen and Ohring (1984) also proposed a method for deriving surface albedo directly from planetary albedo measurements by comparing correlations between zonally averaged NOAA Scanning Radiometer (SR) data (visible planetary) against *prescribed,* zonally averaged, full-spectrum surface albedos. These methods do not account for spectral and angular variations, ozone or H_2O absorption, aerosol absorption, or the wavelength dependence of surface albedo.

Norton et al. (1979) investigated seasonal and interannual (1967–74) variations in Sahelian surface albedo, based on the Applications Technology Satellite (ATS-3) green sensor (0.48–0.58 μm), incorporating simple corrections for Rayleigh scattering and sun-angle effects and avoiding cloudy data using a combination of the minimum brightness technique (see section 4), visual image interpretation, and simulation studies of ATS-3 response to several versions of theoretical cloudiness. Preuss and Geleyn (1980) used Nimbus-3 minimum planetary albedos as input to a radiative-transfer model to produce a global map of yearly mean surface albedo. They developed a linear relationship in which surface albedo is derived as a function of minimum planetary albedo and the clear-atmosphere backscattering and transmissivity terms. These terms were developed for four major ocean and land types in each hemisphere and for one polar snow region.

c. *Why is there still a problem*

All of these studies have contributed to understanding the earth's surface albedo, but this knowledge is not uniformly accurate over the whole globe. In particular, seasonal, spectral and angular dependence information for many vegetation and surface types and for naturally heterogeneous surfaces is not available.

Since a 2% change in planetary albedo is considered significant to climate (see, e.g., Wetherald and Manabe, 1975; Hansen et al., 1984), more careful treatment of systematic atmospheric effects and better characterization of the natural variation of surface types is needed to assure this kind of accuracy in climate models. Monitoring of changes in vegetation also requires accurate removal of systematic effects produced by changes in the atmosphere or viewing geometry in order to isolate changes at the surface itself.

Consideration of what we already know about the factors which control the albedo of vegetated surfaces indicates the complex nature of the problem. The characteristic, spectrally dependent reflectance exhibited by healthy green vegetation has been measured by many researchers (e.g., Billings and Morris, 1951; Olson and Good, 1962; Gates et al., 1965; Knipling, 1970; Hoffman, 1970; Fuller and Rouse, 1979; Brest, 1987); snow-free reflectance is on the order of 5–10% in the visible (<0.7 μm), with a steep rise beyond 0.7 μm to about 30–60%. Seasonally, the rise in full spectrum albedo from the beginning to the peak of the growing season (e.g., spring to summer) (Bauer and Dutton, 1962; Kung et al., 1964; Berglund and Mace, 1972; Ashley and Rea, 1975; Brest, 1987; Pinty and Szejwach, 1985) is the net effect of two opposing trends: the spring–summer trend is governed by stable or decreasing reflectance in the visible and increasing reflectance in the near-IR (0.7–1.1 μm). The summer/rainy season is characterized by a visible reflectance minimum due primarily to chlorophyll absorption at ~0.65 μm, and a near-IR maximum (e.g., Scott et al., 1968; Brest, 1987) variously ascribed to canopy development and layering, and internal leaf structure (Allen and Richardson, 1968; Gausman et al., 1970; Woolley, 1971; Gausman, 1977).

The complex spectral dependence of the reflectance of an individual plant leaf combines with the canopy structure to produce angular dependence of the reflectance that varies with wavelength (Kimes, 1983, 1984; Duggin, 1985). The effects of vegetation, in turn, combine with those of soil/rock surfaces and topography to produce the total effect. Furthermore, the angular and spectral dependence of atmospheric effects may combine nonlinearly with those of the surface. Study of these effects at larger scales is further complicated by the spatial variations of canopy composition and structure.

The presence of snow on vegetated and nonvegetated terrain alters the spectral dependence of the surface reflectance. Snow and ice display a spectral dependence generally opposite to that of vegetation; i.e., high reflectance (70–90%) in the spectral region up to 0.7 μm, and a relatively steep decline to ~30–40% at ~1.1 μm (see, e.g., Grenfell and Maykut, 1977; Swain and Davis, 1978; Wiscombe and Warren, 1981; Warren, 1982). The complementary spectral dependences for vegetation and snow combine to produce large reflectance increases in the visible and smaller reflectance increases or decreases in the near-IR (Brest, 1987). The magnitude of these changes is dependent not only on the spectral reflectances of the vegetation and snow, but also on the height and density of vegetation and age and depth of snow (Kung et al., 1964).

In summary, the reflectances of vegetated surfaces exhibit distinct spectral dependences that vary with vegetation type, season, and snow cover. The additional complexity of the spectral and angular variations of the reflectances suggests the need for caution in inferring full-spectrum albedo from single-channel (narrowband or broadband) observations covering limited time periods or land types. This complicated relation between broadband planetary and surface albedo may not allow use of linear correlation techniques to obtain the latter from satellites unless they are based on a large suite of seasonal and surface-type models (similar to the methods of Preuss and Geleyn, 1980; Briegleb et al., 1986; Taylor and Stowe, 1984, but with more surface types).

Our analyses of the NOAA-5 SR reflectances at 0.6 μm cannot address all of the issues discussed above; however, we can evaluate the magnitude and nature of some atmospheric effects and assess techniques for measuring surface properties from satellites. The expected contrast in 0.6 μm reflectances among different surface types is generally only 5–15%, while the expected seasonal (snow-free) oscillations are only a few percent (Olson and Good, 1962; Gates et al., 1965; Markham et al., 1981; Scott et al., 1968; Brest, 1987). These variation magnitudes are similar to those caused by variations in viewing geometry and canopy structure (Kriebel, 1979; Kimes 1983, 1984), ozone absorption and Rayleigh scattering (see section 3), and radiometer performance so that care must be taken to isolate and remove nonsurface effects. We investigate the pattern of geographic reflectance contrasts and seasonal variations and the variability of reflectances within vegetation groups to assess analysis methods and the land-cover classification itself (see Matthews, 1983, 1985 and Table 1, herein).

3. Magnitude and variation of atmospheric effects

a. Rayleigh scattering

Scattering of sunlight by the atmosphere not only introduces wavelength- and angle-dependent differences between the satellite-measured and surface reflectivities, but also contributes an angle-dependent component to the radiation striking the surface. For dark surfaces (e.g., ocean, vegetated land) the spectral and angular variation of the Rayleigh scattering contribution to satellite-measured reflectances can be comparable to the total contribution of the surface. Consequently, measuring surface-reflectance variations with latitude or season, or over many years using different radiometers with different geometries cannot be

TABLE 1. Descriptions and areas of major vegetation types (Matthews, 1983) used in this study. (Map symbols refer to Figs. 5d and 6c.)

No.	Map symbol	Area ($\times 10^6$ km^2)	Description
1	1	12.3	tropical evergreen rainforest, mangrove
2	2	3.3	tropical/subtropical evergreen seasonal broadleaved forest
3	3	0.2	subtropical evergreen rainforest
4	4	0.4	temperate/subpolar evergreen rainforest
5	5	0.8	temperate evergreen seasonal broadleaved forest
6	6	0.5	evergreen broadleaved sclerophyllous forest, winter rain
7	7	0.5	tropical/subtropical evergreen needleleaved forest
8	8	9.3	temperate/subpolar evergreen needleleaved forest
9	9	3.0	tropical/subtropical drought-deciduous forest
10	A	5.2	cold-deciduous forest, with evergreens
11	B	4.0	cold-deciduous forest, without evergreens
12	C	2.7	xeromorphic forest/woodland
13	D	1.7	evergreen broadleaved sclerophyllous forest
14	E	2.5	evergreen needleleaved woodland
15	F	3.7	tropical/subtropical drought-deciduous woodland
16	G	2.5	cold-deciduous woodland
17	H	1.3	evergreen needleleaved shrubland/thicket, evergreen dwarf shrubland
18	I	0.7	evergreen needleleaved or microphyllous shrubland/thicket
19	J	0.8	drought-deciduous shrubland/thicket, drought-deciduous dwarf shrubland/thicket
20	K	0.5	cold-deciduous subalpine/subpolar shrubland, cold-deciduous dwarf shrubland
21	L	8.9	xeromorphic shrubland/dwarf shrubland
22	M	7.4	arctic/alpine tundra, mossy bog
23	N	6.5	tall/medium/short grassland with 10–40% tree cover
24	O	3.7	tall/medium/short grassland with ≤10% tree cover or tuft-plant cover
25	P	9.4	tall/medium/short grassland with shrub cover
26	Q	0.8	tall grassland, no woody cover
27	R	0.8	medium grassland, no woody cover
28	S	6.1	meadow/short grassland, no woody cover
29	T	0.3	forb formations
30	—	15.6	desert (bare soil)
31	*	16.1	ice
32[1]		17.5	cultivation
Total		149.0	

[1] Cultivated areas not shown on maps.

done accurately without correcting for the systematic effects of Rayleigh scattering. For example, since the NOAA-5 Scanning Radiometer spectral response peaks near 0.6 μm (Fig. 1), the seasonal oscillation of the reflectance of a midlatitude location with a surface spectral albedo of 0.10 would appear to be about one-quarter its annual mean value due to Rayleigh scattering variations with solar zenith angle. Another radiometer, with a spectral response peaking 0.1 μm lower or higher than NOAA-5 SR, would detect a "seasonal" variation of about 50 or 15%, respectively (see also Duggin, 1985). For very bright surfaces, especially snow- and ice-covered surfaces, the contribution from Rayleigh scattering is a smaller fraction of the total, but the larger role of multiple scattering between the surface and atmosphere can make the spectral and angular dependence stronger. Monitoring of high-latitude surface spectral reflectances is especially difficult because of the large average solar zenith angles; the effective optical depth for Rayleigh scattering at the summer pole is about 0.15 for the NOAA-5 effective wavelength.

Rayleigh scattering effects are removed in our analysis by comparing measured radiances to model-calculated radiances as a function of viewing geometry and surface spectral reflectance. The model radiances are calculated for a single wavelength (0.6 μm) using an invariant imbedding technique (Sato et al., 1977); the Rayleigh optical depth is weighted by the solar spectrum and the NOAA-5 SR spectral response (Rossow et al., 1987) and equals 0.063. The retrieved surface reflectance value is for a Lambertian surface; however, the value also represents the correct value of the surface bidirectional reflectance at a particular geometry within about 1–2% for surface albedo <50%. The error in the angular distribution of the multiple-scattered radiation only becomes significant for ice- and snow-covered surfaces; however, such surfaces exhibit nearly isotropic reflectance except for a specular component over limited ranges of solar zenith angle (Warren, 1982; Taylor and Stowe, 1984). Higher accuracy for all surfaces can be obtained by an iterative analysis that explicitly incorporates the bidirectional surface reflectances inferred from the previous retrieval into a second analysis of the same data. Overall, the uncertainty of surface reflectances contributed by the Rayleigh correction procedure is ≤1%.

b. Ozone

Atmospheric ozone has a weak absorption band between 0.5–0.6 μm. Ozone effects reduce satellite-measured radiances in the visible, in proportion to increasing pathlength and ozone abundance. The absorption is incorporated in the monochromatic model calculation by an absorption coefficient averaged over the absorption band and weighted by the SR spectral response and the solar spectrum, including the spectral shift of Rayleigh scattering (Lacis and Hansen, 1974).

Because of a code error, ozone corrections were not made to these data during the initial data processing but were made later to the averaged monthly reflectances. Ozone transmissions are calculated as a function of the sun-target pathlength (i.e., cosine of solar zenith angle, μ_0), satellite-target pathlength (i.e., cosine of satellite scan angle, μ), and zonal, monthly mean column ozone abundance (O_3) for 1977 (from Hilsenrath and Schlesinger, 1981).

Because monthly reflectance at each location was an average of three or four values retrieved throughout the month with slightly different solar zenith angles, ozone abundances and satellite scan angles, we could calculate only approximate monthly ozone-transmission corrections. First, solar zenith angles (SZA) for 0930 local standard time (see Robock and Kaiser, 1985) were calculated for the midday of each month to approximate the average solar zenith angle at higher latitudes where the ozone effect is largest (see Fig. 3). However, conditions on the last day of the month were considered more representative of retrieval conditions in January, since high northern latitudes are insufficiently illuminated in the morning to provide observations until the end of the month.

Since satellite-target pathlength only varies by a factor of 2, its effect on transmissions is relatively minor; for all latitudes and months, the twofold increase in satellite-target pathlength reduced transmission by <0.028 (e.g., from 0.928 to 0.900). The transmissions used for ozone corrections in this study are approximated by those for the average satellite-target pathlength ($\mu = 0.75$). The largest effect on total pathlength is from the large variations in solar zenith angle encountered throughout the year. For the morning observation time, sun-target pathlength varies by a factor of 6 with season and latitude (μ_0 from 0.15 to 0.825). (The application of ozone corrections was constrained to locations with 0930 SZA of <82°; values at all other locations were neglected.)

Figure 2 shows 5 months of latitudinal values of 0930 SZA (dotted line), O_3 abundance (dashed line), and ozone transmissions (solid line). The correlation of large O_3 abundance and solar zenith angles makes the latitudinal dependence of the ozone effect highly nonlinear: the effect is small and nearly constant over low- to mid-latitudes, but rapidly increases towards higher latitudes. Minimum SZA occurs in the southern subtropics in January, shifting to the northern subtropics in July. The relatively flat tropical/subtropical O_3 minimum oscillates between 200–250 Dobson Units (D.U.) during the year. In these low latitudes, where the SZA and O_3 minima generally coincide, transmissions are high (0.95) and corrections are small. High latitude (50°–60°) O_3 concentrations peak in late winter/early spring (400–500 D.U. in the Northern Hemisphere in February and April; 300–400 D.U. in the Southern Hemisphere in October) at nearly the same time that SZA is large. Transmissions as low as 0.80–0.90 are apparent in high-latitude winter and spring months. In several high-latitude cases where the O_3 and SZA trends diverge (e.g., northern latitudes in July, southern latitudes in January, February, April and October), the effect of declining or stable ozone abundance, which would tend to increase or stabilize transmissions, is overridden by the effect of increasing SZA.

The sensitivity of the satellite-derived surface reflectances to the correction for ozone absorption is demonstrated in Fig. 3, in which differences between corrected and uncorrected zonal mean land reflectances are plotted for 5 months. Transmissions are highest primarily in low-latitude, low reflectance regions, resulting in corrections that are small in magnitude (~1%) and essentially constant over the whole year. However, in high latitudes where bright reflectances, high ozone abundance and large solar zenith angles often coincide, atmospheric ozone absorption, if unaccounted for, can produce zonal reflectances as much as 15% (absolute magnitude) too low. Point-location reflectances may be underestimated by as much as 20%. Failure to correct for ozone absorption would thus lead to a systematic underestimate of the magnitude of the snow albedo feedback estimated from satellite data, as well as producing a spurious seasonal cycle in snow-free areas. The uncertainty introduced by our approximate treatment of ozone effects is as much as 3–5% for the brighter surfaces at very high latitudes; however, proper corrections can reduce this uncertainty to the much smaller values produced by variations in O_3, if a climatology is used, or in measuring O_3, if operational satellite observations are used (Rossow et al., 1987).

c. *Cloud contamination*

The average reflectance of a small area of cloud is generally so much greater than that of the surface that even a small amount of cloud contamination can significantly alter satellite-measured radiances. Many schemes have been proposed for obtaining cloud-free radiances from satellite images, but the wide variety of cloud types and climatological situations can foil simple, even though very strict, tests. Specific methodologies and validation test results are discussed in section 4. Several especially difficult situations are highlighted here: regions of extraordinarily persistent cloudiness, snow-covered/snow-free boundary regions, and polar regions. Portions of tropical land areas appear to be completely covered by thin cirrus or low, broken cumulus for periods of >30 days during certain seasons, as indicated by higher than expected reflectances, anomalously cold temperatures and large seasonal oscillations in reflectance, and geographic patterns in the anomalies that are uncorrelated with surface characteristics. Figure 4a shows surface-reflectance differences between October and April for Africa. (The data have been averaged to 1° latitude/1° longitude resolution.) Reflectance values along the western coast, which is

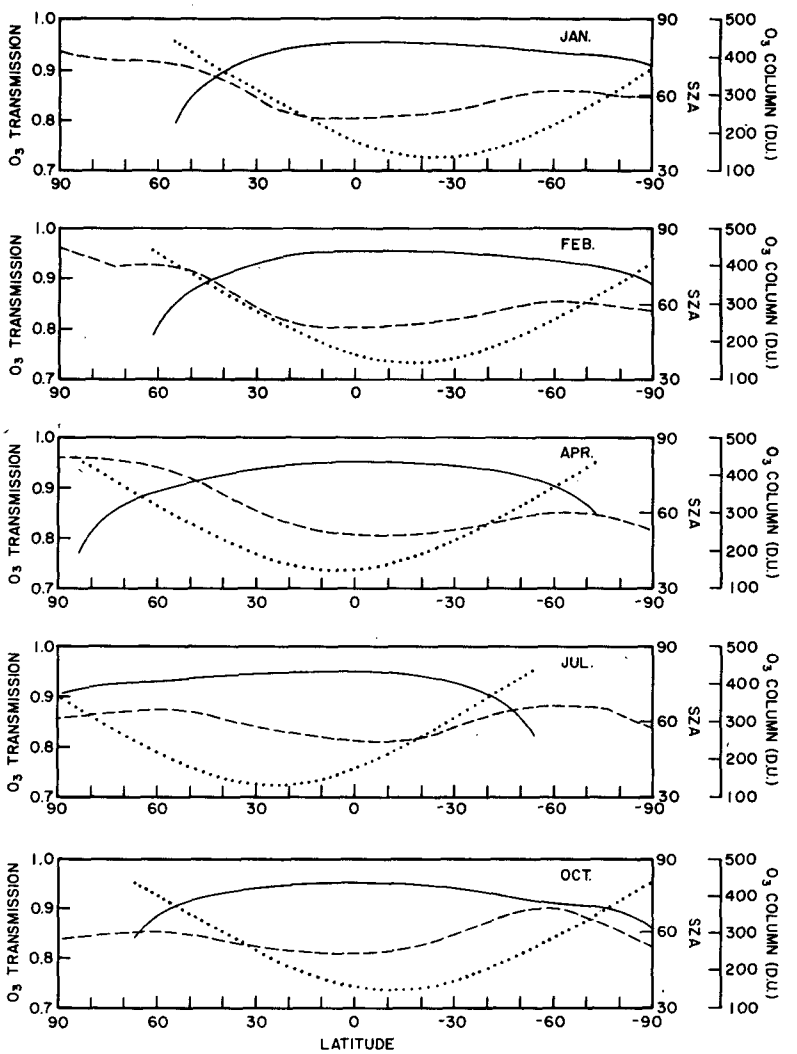

FIG. 2. Solar zenith angle (dotted line), ozone column abundance (O_3) (dashed line) and ozone transmission (solid line) for January, February, April, July and October, 1977.

occupied by tropical evergreen rainforest and evergreen seasonal forest, would be expected to be 10% or less, with seasonal oscillations <5%. Seasonal variations, in fact, range up to more than 15% (Fig. 4a). Monthly reflectance histograms for African tropical rainforests (Fig. 4b) display modes between 6–10%, consistent with expected reflectances; however, secondary peaks above 20% in July and October suggest the presence of cloud contamination in the data. Temperatures contemporaneously derived from the NOAA-5 thermal channel (including correction for water vapor absorption, see Rossow et al., 1987) appear to be anomalously low in these regions in July and October, further suggesting cloudy conditions: derived temperatures are 12°–17°C, while long-term surface station temperature records suggest seasonally stable temperatures closer to 25°–28°C in these locations. April appears to be the clearest month while October is the cloudiest month. These coastal areas also show anomalously high albedos in several other studies, based on satellite data sets covering varying time periods and spectral ranges (Raschke et al., 1973; Rockwood and Cox, 1976; Norton et al., 1979; Raschke and Preuss, 1979).

South America also exhibits unexpectedly high reflectances and large reflectance oscillations over tropical rainforest areas, with a maximum in February and a minimum in July. As in Africa, these anomalous locations generally coincide with cold temperature anomalies. Reflectance histograms for South American rainforests, while consistently wider than those for Africa, display mode values of 4–10% throughout the year, accompanied by brighter values up to ~20% in all months except July; temperatures in the high reflectance areas are ~15°–17°C. The homogeneity of

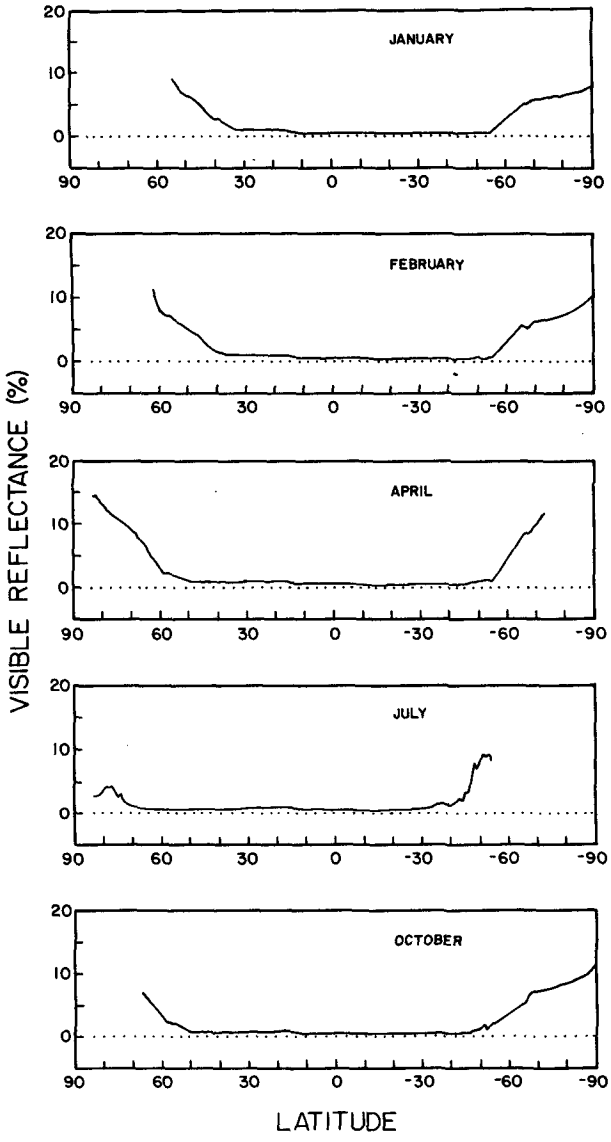

FIG. 3. Magnitude of ozone corrections (in absolute percent) in zonal mean visible surface reflectance. Ozone-corrected minus uncorrected reflectance (land only) is plotted by latitude for the 5 months of analyzed NOAA-5 SR data.

July reflectances found throughout the basin is accompanied by July temperatures of 25°–27°C, consistent with station temperature data. The large seasonal variations in reflectance and temperature, together with rainforest reflectances two to three times those anticipated and temperatures 10°C lower than expected, indicate that the mean monthly reflectances were cloud-free only 1 month out of the 5. Similar indications of local cloud persistence in South America, in the form of high-reflectance anomalies, can also be found in the results of Raschke et al. (1973), Raschke and Preuss (1979), Preuss and Geleyn (1980), and Briegleb et al. (1986).

Accurate monitoring of seasonal or long-term variations in tropical vegetation from satellites may be very difficult because of this persistent cloudiness. Most cloud-removal schemes depend on the relatively higher variability of cloudy scenes compared to cloud-free scenes; however, the tropical cloudiness illustrated here requires a different approach to identify infrequent clear-sky occurrences.

Snow-melt zones are regions where surface reflectances are nearly as variable in time and space as clouds, making proper separation of clear and cloudy scenes very difficult (see Rossow et al., 1987). Polar regions are more difficult because the effect of cloudiness on satellite-measured reflectance can be positive or negative depending on cloud optical thickness, surface albedo and viewing geometry (Rossow et al., 1987).

d. Other atmospheric effects

For the NOAA-5 SR spectral response, the only gaseous effects that need to be considered are Rayleigh scattering and ozone absorption; however, observations in other parts of the solar spectrum are affected by other gaseous absorptions (Duggin, 1985; Vulis et al., 1987). The most variable absorbing gas is water vapor,

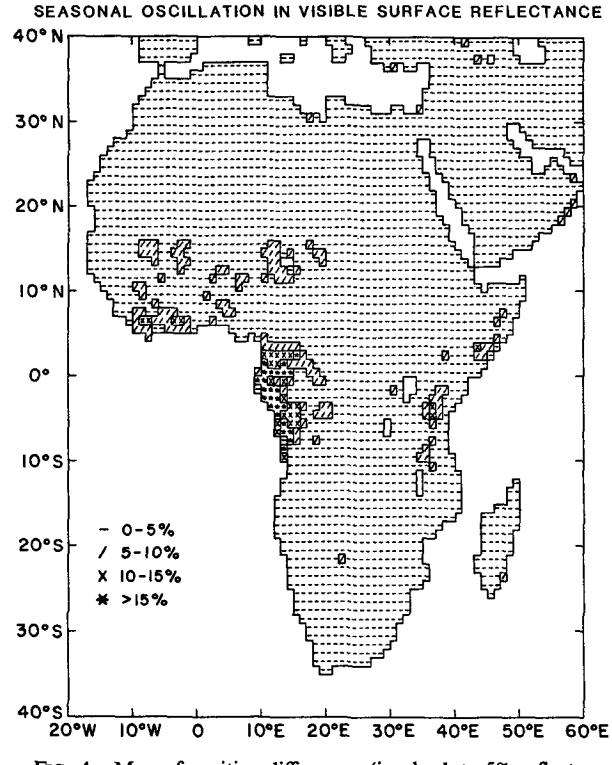

FIG. 4a. Map of positive differences (in absolute 5% reflectance intervals) between October and April shows the seasonal oscillation in visible surface reflectance for Africa. Large oscillations (>10%) along the western equatorial coast, occupied by evergreen rainforests, originate from anomalously high October (cloudy) reflectances. (25 km resolution NOAA-5 data averaged to 1° resolution.)

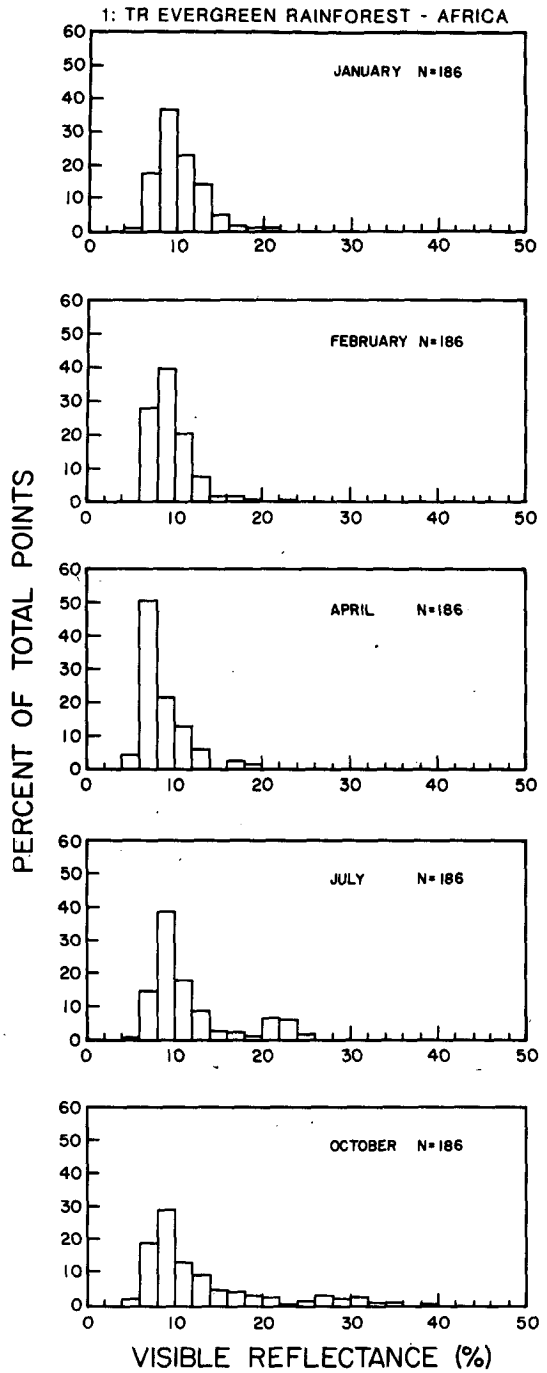

FIG. 4b. Monthly visible reflectance histograms for tropical rainforests (No. 1 in Table 1) in Africa. Mode values are between 6 and 10% in all months. July and October exhibit bright reflectance values trailing above 20%, indicating residual cloud contamination. Note that the number of total (N) points is for 1° cells in this and all subsequent histograms.

which has several bands in the near-infrared portion of the solar spectrum.

Satellite observations of the surface throughout the solar spectrum are also affected by the background distribution of aerosols present even in cloud-free locations. Concentrations of such aerosols are found in the lower stratosphere, but more importantly in the boundary layer and lower troposphere. Estimates of the optical depth of such aerosols (Toon and Pollack, 1976) suggest a scattering effect comparable to Rayleigh scattering over land at 0.6 μm; however, the weaker wavelength dependence of aerosol scattering means that aerosol scattering predominates at near-infrared wavelengths (Vulis et al., 1987). Some absorption of sunlight by aerosols is also possible (Toon and Pollack, 1976). Systematic variations in aerosol abundances are not well known; hence, the *average* effect of aerosols on satellite radiances must be included with *surface* reflectance for now. Aerosols are probably the largest source of uncertainty in removing atmospheric effects from satellite data to determine actual surface albedo, other than radiometer calibration.

4. Methodology

Obtaining an accurate measure of surface spectral reflectance (and, ultimately, surface albedo) from satellite data requires an analysis to identify cloud-free observations, remove other effects on the satellite-measured radiances, and account for radiometer noise or the natural variability of surfaces. Inability to correct for certain atmospheric or surface effects may require additional procedures to eliminate or minimize these unknown factors. We have discussed the corrections applied to the measured radiances for Rayleigh scattering and ozone absorption in section 3; here we describe the technique for identifying cloud-free measurements, assess its success, and evaluate the magnitude of other effects that are only partially accounted for in this analysis.

a. Minimum radiance method

A common procedure for identifying cloud-free measurements is to examine a time series of measurements for each location and take the absolute minimum radiance to represent cloud-free conditions[1] (e.g., Pinty and Szejwach, 1985; Norton et al., 1979). The primary difficulty with this approach is that, over the time periods generally required to insure the occurrence of at least one cloud-free situation (5–15 days), many other effects occur which can produce darker reflec-

[1] A more common "analysis" procedure is to examine satellite images visually for the presence of clouds. This procedure is, in some ways, a qualitative version of the minimum radiance method, although texture and other pattern information provide additional clues to the presence of clouds. However, the lack of control of film and emulsion characteristics makes the reliable detection of thin cirrus and some broken cloudiness by this method very uncertain. Also, quantitative accuracy is difficult to assess. In any case we are only considering automated image-analysis techniques that make possible global and annual surveys of surface reflectance at relatively high temporal and spatial resolutions.

tances than are characteristic of the surface. Actual variations in surface conditions, such as wetness or vegetation structure changes, introduce natural variability of the surface reflectance. Navigation uncertainties cause motion of the image pixels with respect to fixed locations, thereby producing an intrinsic variation of measured radiances for inhomogeneous surfaces. Broken clouds casting shadows or variations in illumination geometry, if not accounted for, introduce further variations. Use of a single value retains all of the uncertainties caused by atmospheric and radiometer "noise." Additionally, the more samples examined, the more probable an extreme variation in radiometer performance. For example, the 2% rms noise level estimated for the NOAA-5 SR represents the interval containing ~67% of the observations of a constant target; however, more extreme deviations are more likely with larger sample sizes. Thus, use of the absolute minimum of a large number of samples as the cloud-free radiance causes increased sensitivity to "rare" events and a bias towards lower values.

A second difficulty with the minimum radiance approach is that this value may actually represent cloudy conditions over bright surfaces for certain viewing geometries. This effect is a consequence of the different angular distribution of solar radiation reflected from clouds and rough surfaces.

The magnitude of these effects was inferred in this study from comparisons of the minimum and mode radiances with the whole distribution of radiances occurring during a month. Distributions were formed representing small geographic regions (~100 km square), and representing similar vegetation and soil type classifications over the whole globe. The whole ocean distribution represents a larger statistical sample of a more homogeneous surface. Most of these distributions exhibited a characteristic shape, illustrated by the example in Fig. 4b: the mode and values near the mode represent the generally less variable cloud-free radiances while the extended bright tail represents the more variable cloudy radiances. Collection of such distributions over progressively longer time periods shows a systematic increase in the difference between the absolute minimum and the mode, with no change in the mode value. For 15–30 day time records, radiometer noise and atmospheric variations alone produce minimum radiance values about 3–5% lower than the mode value.

b. *New method*

The basic objective of this new method is to obtain a few samples of cloud-free radiances for each site representing the distribution of reflectance values about the mode in histograms like those in Fig. 4b. To avoid the bias introduced by using the absolute minimum radiance and to reduce the uncertainty from radiometer and atmospheric variations which are quasi-random, we average the four visible surface reflectances[2] corresponding to the four warmest infrared brightness temperatures occurring in one month. A similar procedure can also be used to obtain cloud-free infrared radiances, reversing the roles of the two channels (Rossow et al., 1987). Comparisons were made among this average value, the average values obtained with larger and smaller sample sizes, the minimum value, and the mode of the full distribution: for most situations, the uncertainty in this estimate of the mode reflectance is $\leq$2%.

Several additional tests are performed to eliminate remaining cloud contamination and detect snow cover (Rossow et al., 1987). Examination of the reflectance histograms from a 1-month period shows that the variation about the mode value is generally smaller than the variations produced by cloudiness. This fact is even clearer if histograms of similar surface types are formed only from the four reflectances corresponding to the warmest infrared brightness temperatures (see, e.g., Fig. 4b): distribution widths are generally much less than 10%. Thus, the standard deviation of the four reflectance values *for each site* (defined by the data resolution to be ~20 km square areas) is required to be <5%; if the standard deviation is larger, the reflectance corresponding to the coldest brightness temperature is discarded. If the standard deviation is still too large, no result is reported for that location. Persistently cloudy regions are generally detected by the failure of this test. However, as discussed in section 3c, some tropical regions exhibit persistent cloudiness with sufficiently constant properties to pass the test, even when applied to a 30-day record, suggesting that a proper measure of surface reflectance may be obtainable for some tropical regions only by analysis of 3–6 months of data.

A second test for cloud contamination is applied to the average reflectances. Using digital vegetation (Matthews, 1983, 1985) and soil (Oxford Atlas, 1973) data (Tables 1 and 2) for all locations, we constructed reflectance histograms for all major vegetation/soil classes as a function of latitude and month. For those locations belonging to classes with sufficiently narrow histograms (standard deviations $\leq$5%), the average reflectance is required to be within −4% and +7% of the class mode value, unless snow is present. For those locations belonging to more heterogeneous classes (i.e., sparse, arid land types, generally confined to low latitudes), this test is not performed.

A reflectance value that is larger than its class mode value is retained if it is consistent with the presence of snow. Three conditions are required: 1) the associated average surface temperature determined from the four

[2] Each visible radiance is converted to a surface reflectance by comparison of the observed radiance to the model calculated radiance as a function of viewing geometry, ozone abundance and surface spectral albedo. As noted in section 3, the ozone correction was inadvertantly left out, requiring later correction.

TABLE 2. Descriptions and areas of major soil types (digitized from Oxford World Atlas, 1973) used in this study. (Map symbols refer to Fig. 6d.)

No.	Map symbol	Area ($\times 10^6$ km^2)	Description
			Entisol
			Weakly developed, shallow soil on freshly exposed rock or alluvium without pedogenic horizons.
1	1	0.9	Aquent: seasonally or perennially wet
2	2	2.9	Orthent: loamy or clayey texture, often shallow to bedrock
3	/	7.0	Psamment: sand or loamy sand texture
			Vertisol
			High active clay content, swells when wet and cracks when dry; moderate to high nutrient status.
4	4	0.1	Udert: usually moist; cracks open less than 90 days/year
5	5	2.1	Ustert: dry and cracked more than 90 days/year
			Inceptisol
			Moderately developed with some pedogenic alteration; usually moist; medium to high base supply.
6	6	0.7	Andept: amorphous or allophanic clay present, often associated with volcanic ash or pumice
7	7	10.2	Aquept: seasonally or perennially wet
8	8	1.1	Ochrept: soil with thin light-colored surface horizons
9	9	0.9	Tropept: continuously warm or hot
10	+	0.2	Umbrept: dark surface horizons; medium to low base supply
			Aridisol
			Desert or saline soil with pedogenic horizons; poor in organics; nutrient content often high except for nitrogen; usually dry more than 6 months/year.
11	−	22.5	Aridisol: undifferentiated
12	(	2.2	Argid: clay-accumulation horizons
			Mollisol
			Brown forest, chernozem, or chestnut soil; dark, organic-rich surface horizons; high base supply; either usually moist or usually dry.
13	&	0.4	Alboll: soil with a seasonally perched water table
14	%	5.1	Boroll: cool or cold
15	$	0.2	Rendoll: subsurface accumulation of calcium carbonate; no clay
16	#	1.2	Udoll: temperate or warm; usually moist
17	?	4.1	Ustoll: temperate to hot; dry more than 90 days/year
18	>	0.5	Xeroll: cool to warm; moist in winter, continuously dry for more than 60 days in summer
			Spodosol
			High latitude podsol; subsurface accumulations of amorphous materials (iron, aluminum); usually moist or wet; strongly leached; poor in mineral elements; acidic; structureless.
19	<	4.1	Spodosol: undifferentiated
20	=	0.1	Aquod: seasonally wet
21	@	0.2	Humod: subsurface accumulations of organic matter
22	A	1.2	Orthod: subsurface accumulations of organic matter, iron and aluminum
			Alfisol
			Mid-latitude podzolic and degraded grassland soil; grey to brown surface horizons; subsurface clay accumulations; medium to high base supply.
23	B	4.9	Boralf: cool
24	C	3.3	Udalf: temperate to hot; usually moist
25	D	8.6	Ustalf: temperate to hot; dry more than 90 days/year
26	E	1.4	Xeralf: temperate to warm; moist in winter; continuously dry for more than 60 days in summer

TABLE 2. (*Continued*)

No.	Map symbol	Area ($\times 10^6$ km^2)	Description
			Ultisol
			Strongly weathered or podzolic soil; subsurface clay accumulations; usually moist; low in organic matter; low base supply.
27	F	0.5	Aquult: seasonally wet
28	G	0.3	Humult: temperate to warm; moist all year; high content of organic matter
29	H	5.4	Udult: temperate to hot; usually moist
30	J	1.2	Ustult: warm to hot; dry more than 90 days/year
			Oxisol
			Strongly weathered soil of mid- to low latitudes; (laterites, latosols); deep and porous; pedogenic horizons with mixtures of kaolin, hydrated oxides, and quartz; low in weatherable materials.
31	K	7.6	Ortox: hot; nearly always moist
32	L	3.7	Ustox: warm or hot; long dry periods; moist more than 90 days/year
			Histosol
			Bog and peat soils.
33	M	1.3	Histosol: wet organic soil; accumulations of peat or raw humus
			Mountain soil
34	N	10.9	Cryic great groups
35	O	0.3	Boralfs and cryic great groups
36	P	6.9	Udic great groups
37	Q	1.7	Ustic great groups
38	R	2.0	Xeric great groups
39	S	2.0	Torric great groups
40	T	1.2	Ustic and cryic great groups
41	U	0.4	Aridisols; torric and cryic great groups
42	*	16.1	Ice field and glacier
43	W	0.1	Lithosol continuous hard rock within 10 cm of surface
44	|	1.7	Mountain soil < 10 cm, associated phase of rock debris
Total:		148.7	

largest infrared radiances is <273 K, 2) the location is "above" (latitude, altitude) the climatological snow-line position and 3) the average reflectance is >35%. The last condition can eliminate some snow-covered locations, but only those which are relatively variable in space and time. Less variable regions that are mostly snow-covered, but darker than 35% reflectance, are detected successfully because their class histogram in that latitude zone is relatively narrow but shifted towards larger reflectances.

c. *Assessment of the method*

The retrieval analysis fails to obtain any surface-reflectance value in two types of land regions: near the snow-melt line where reflectances vary rapidly during a month, and in some parts of the tropics where cloudiness can persist for a whole month. Both of these cases represent situations that are either very ambiguous or rapidly varying, often because of persistent cloudiness, and comprise approximately 10% of the global land surface area (Rossow et al., 1987). The surface reflectances for smaller gaps (<200 km square) are filled in by interpolation of nearby results for the same surface type.

Several tests (see Rossow et al., 1987, for more details) were performed to verify the reality of the spatial variations obtained in the five monthly reflectance maps resulting from this analysis (Fig. 7). Comparisons of single, manually selected, cloud-free images of several desert, forest and snow-covered regions with the monthly results confirmed an excellent correspondence (correlations >0.7 for 200–300 km regions) for all snow-free regions and for persistently snow-covered regions (such as Siberia and northern Canada). However, the reflectances nearer the snow-melt line showed no correlation to the spatial pattern in a particular image; nevertheless, the area-average values appeared representative of a time-averaged reflectance with a small dark bias caused by the use of the warmest surface temperature observations in the retrieval (Rossow et al., 1987).

Additional regional comparisons focused on the correspondence between geographic boundaries in the seasonal reflectance distributions and vegetation and soil types. The four African maps in Fig. 5 show surface

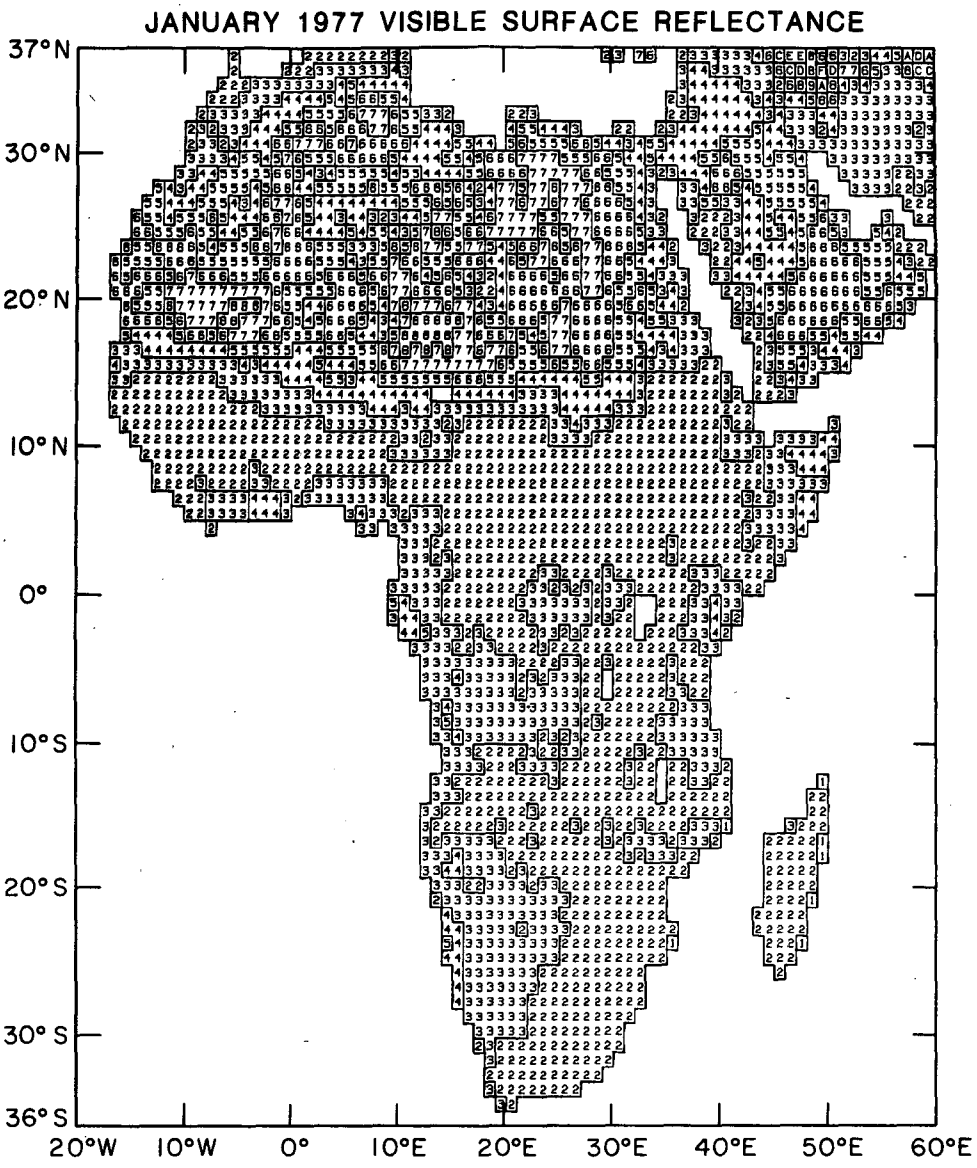

FIG. 5a. January 1977 visible surface reflectance for Africa. Data are mapped at 1° resolution and 5% reflectance intervals: 1 = 5%, 2 = 10%, 3 = 15%, 4 = 20%, 5 = 25%, 6 = 30%, 7 = 35%, 8 = 40%, 9 = 45%, A = 50%, B = 55%, C = 60%, D = 65%, E = 70%, F = 75%, G = 80%, H = 85%, I = 90%, J = 95%, K = 100%.

reflectance (5% intervals) for January (a) and February (b), absolute differences (2% intervals) between the two months (c), and major vegetation types (d). In the western region near ~15°N, well-defined latitudinal reflectance boundaries are apparent in the 2 months shown, as well as in all other months. While we can conclude that progressively brighter reflectances coincide with increasingly arid conditions and sparser vegetative cover, going from the south equatorial coast to the northern Sahara, we cannot conclude that the reflectance boundaries are exactly correlated with the vegetation boundaries mapped in Fig. 5d. The major difference between January and February is the expansion of the 15% boundary (symbol 3) and the corresponding contraction of the 10% boundary (symbol 2) in the southwest region. This shift, resulting from reflectance changes of ~2–4% (Fig. 5c), seems to coincide with a soil boundary, and is perhaps strengthened by effects contributed from vegetation changes, dust storms and, in the south equatorial coast (5°N), from cloud contamination. For more densely vegetated areas, these seasonal oscillations agree with those expected (section 2c).

A similar comparison for Australia is shown in Fig. 6. Due to the predominance of deserts and other arid, sparse, land-cover types in this region, surface reflec-

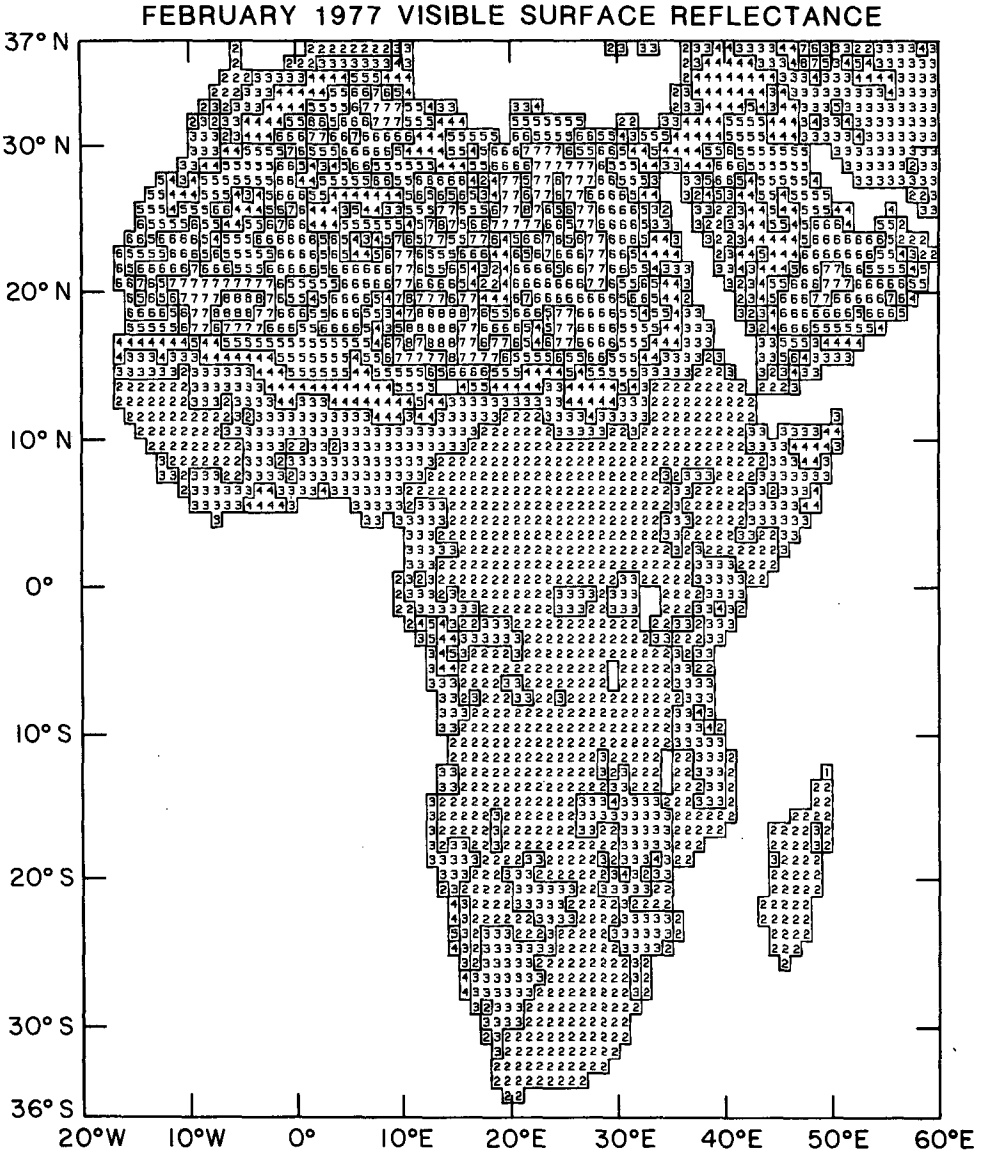

FIG. 5b. February 1977 visible surface reflectance for Africa. Map symbols same as those for Fig. 5a.

tance is controlled primarily by soil color. We therefore expect seasonal oscillations to be small, but we can not anticipate the value of these seasonally stable reflectances. Surface reflectance is mapped in 5% intervals for January (Fig. 6a); absolute differences between January and April are shown in Fig. 6b; vegetation types in Fig. 6c; and soil types in Fig. 6d. The continent is surprisingly dark and is seasonally stable as expected. Most areas are between 5–10% reflectance (symbol 2), and the remaining areas are 10–15% (symbol 3) (Fig. 6a); for the most part, seasonal oscillations are $\leq 2\%$ (Fig. 6b). With the exception of bright regions in the west central, which generally coincide with the western deserts (Fig. 6c) and shallow sandy soils (No. 3, Table 2 and Fig. 6d), vegetation boundaries are indistinguishable in the spatial patterns of reflectance because most vegetation types are sparse and soils are not well correlated with vegetation types. However, the seasonal persistence of reflectance patterns in Australia, produced by regional contrasts $\leq 5\%$, provides circumstantial evidence that the retrievals must be accurate to within 2%, otherwise the patterns could not persist. If uncertainties were >2%, the difference map (Fig. 6b) would appear "noisier", with larger differences. This argument does not insure similar accuracies if the surface, itself, is more variable, only that the analysis method does not introduce larger errors.

Another check on the results is the shape of the histograms of surface reflectances collected for vegetation/soil classes. Several factors can contribute to the dis-

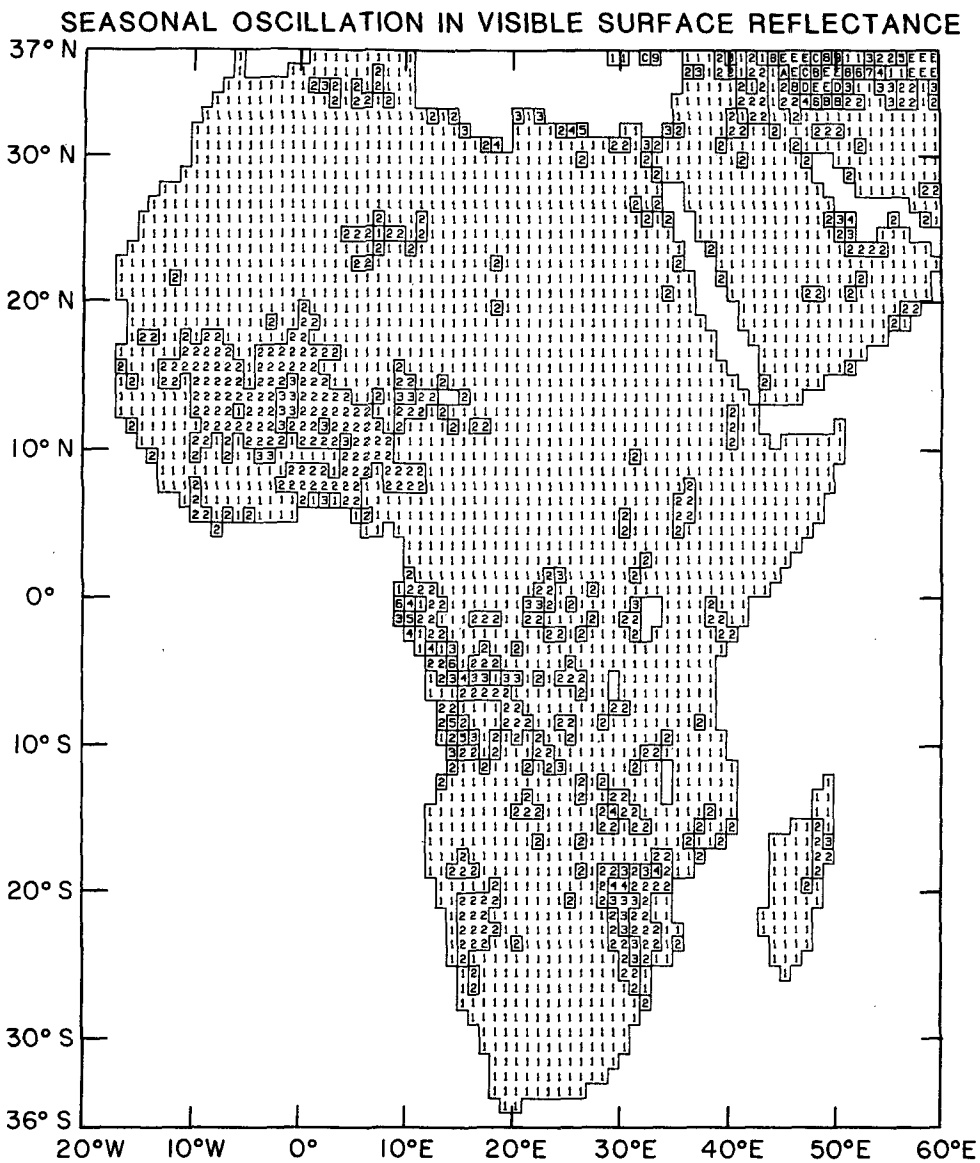

FIG. 5c. Seasonal oscillation in visible surface reflectance for Africa. Positive differences (in absolute percent) between January and February are mapped at 1° resolution and 2% reflectance intervals: 1 = 2%, 2 = 4%, 3 = 6%, 4 = 8%, 5 = 10%, 6 = 12%, 7 = 14%, 8 = 16%, 9 = 18%, A = 20%, B = 22%, C = 24%, D = 26%, E = >26%.

persion of reflectance values about some mode value for each surface class: 1) natural spatial variation of the properties of a class, 2) actual variations of surface conditions with time, 3) unaccounted for variations in atmospheric conditions (primarily aerosols and cloud contamination), 4) unaccounted for angular variations in surface reflectance, 5) radiometer noise and 6) misclassification of a particular location. Further studies are required to separate these effects (see section 6), but if we assume that the total dispersion in the class histograms is due entirely to errors (factors 3, 4, 5 and 6), then we have some measure of the uncertainty in the reflectance values. The shapes of the histograms alone (Fig. 4b and section 5) suggest errors <5%. However, the geographic patterns exhibited in the maps (as discussed above), together with the correspondence of increased histogram dispersion with more heterogeneous (i.e., sparser) vegetation types (see section 5), suggests that the uncertainties must be smaller than this estimate; otherwise, these correlations and patterns would be eliminated. In section 5, we discuss these results with the preliminary assumption that errors are smaller than the observed dispersions.

Further development of such indirect statistical tests is necessary to validate satellite measurements, because we lack direct data on some atmospheric conditions

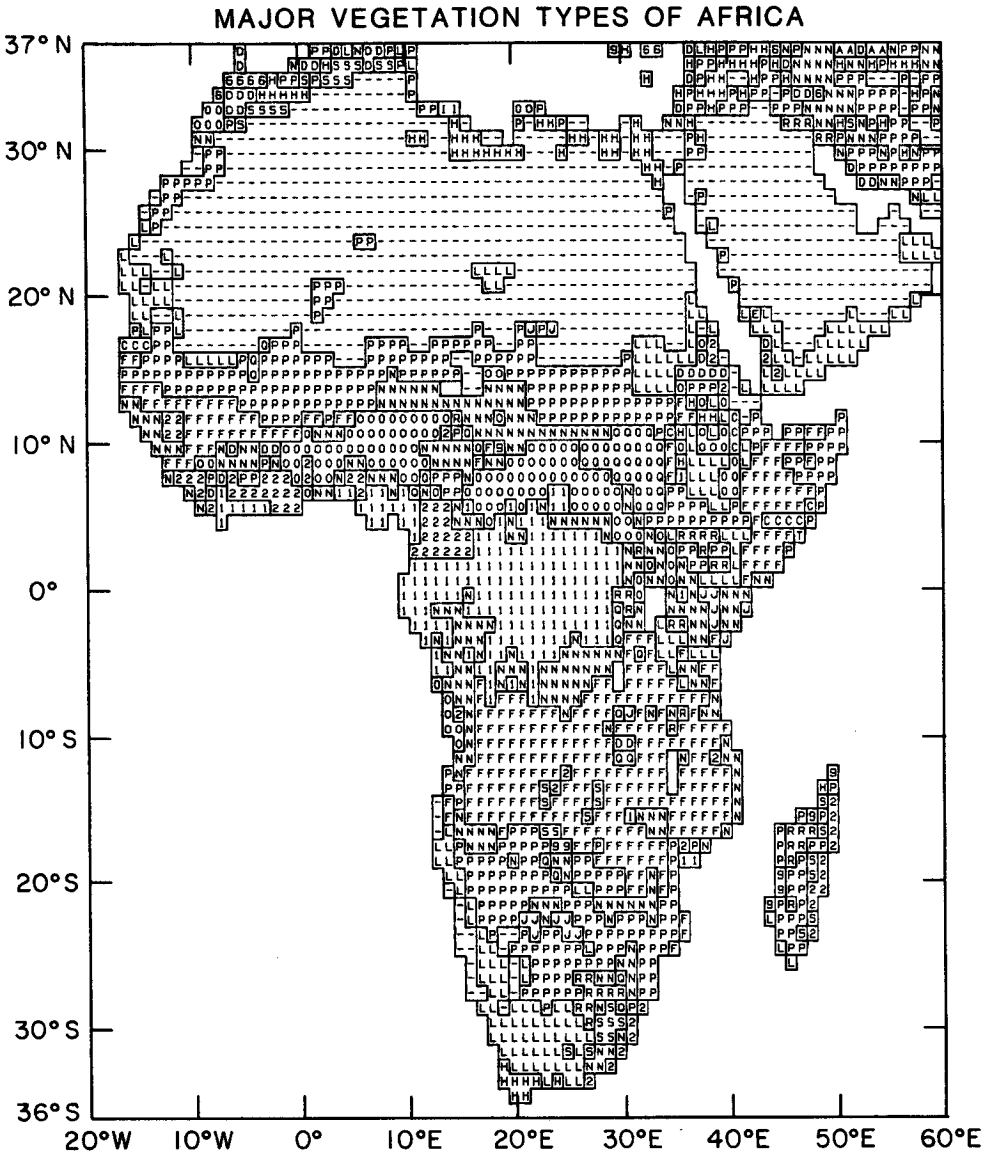

FIG. 5d. Major vegetation types of Africa (Matthews, 1983, 1985). See Table 1 for descriptions and explanation of symbols.

(primarily aerosols) and because little relevant information about surface spectral reflectances over large-area, natural surfaces exists from surface and aircraft sources. We have compared the class-histogram mode reflectances with available information (compiled by Matthews, 1984) and find *qualitative* agreement. This check insures that our values are "reasonable" but cannot usefully constrain uncertainties further.

5. Results

a. Global seasonal reflectance

Fig. 7a–e shows the series of five maps of mean monthly visible surface reflectance derived from the NOAA-5 SR data. Sharp winter gradients in mid- and high latitudes of the Northern Hemisphere follow the snow line (see Rossow et al., 1987, for verification) and move northward during the year until July, when most northern continental areas are relatively homogeneous at $\leq 10\%$ reflectance. (Since ocean reflectance values are typically 2–4%, the land areas of earth in summer are, at their darkest, still two–four times brighter than the ocean at 0.6 μm.) Northwest–southeast trending gradients in North America, most prominant in winter and spring between 40°–60°N, but still apparent in higher resolution maps in July, follow boundaries of dark evergreen forests changing northward through cultivated lands to less dense woodlands and eventually

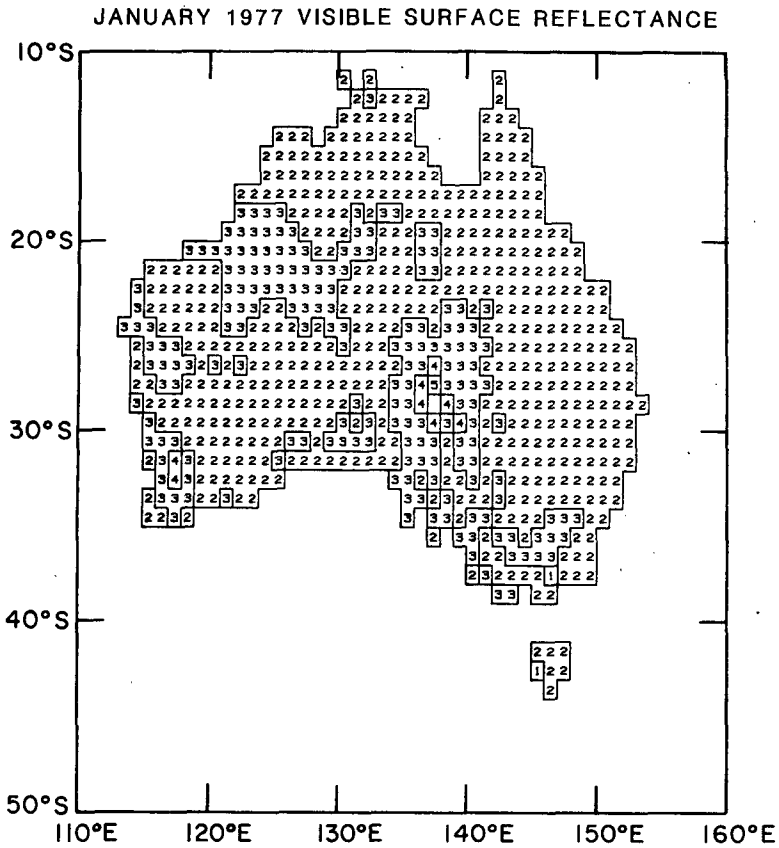

FIG. 6a. January 1977 visible surface reflectance for Australia. Map symbols same as those for Fig. 5a.

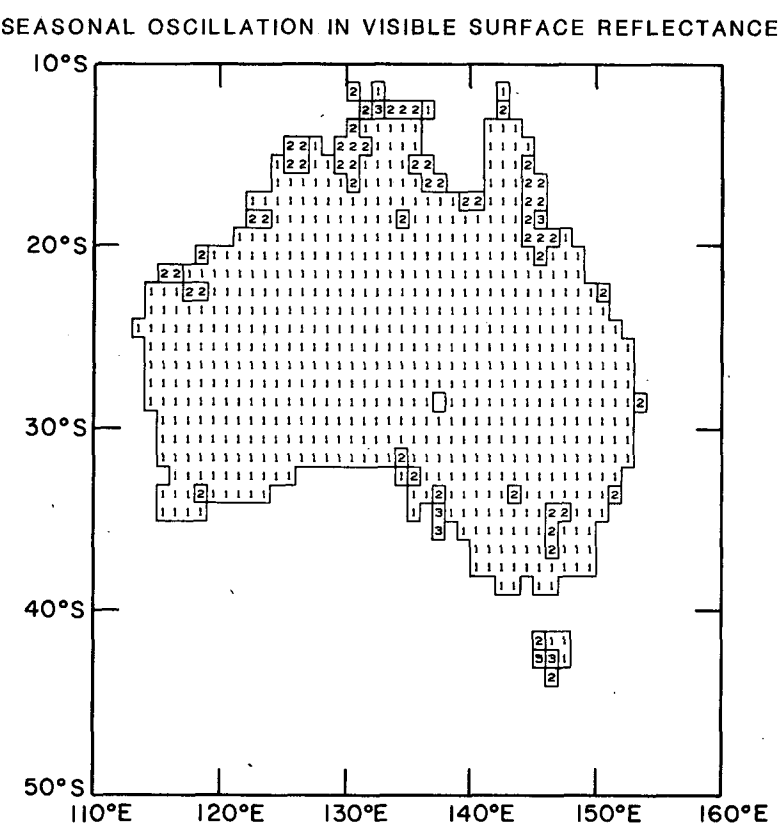

FIG. 6b. Seasonal oscillation in visible surface reflectance for Australia. Positive differences (in absolute percent) between January and April are mapped at 1° resolution and 2% reflectance intervals. Map symbols same as those for Fig. 5c.

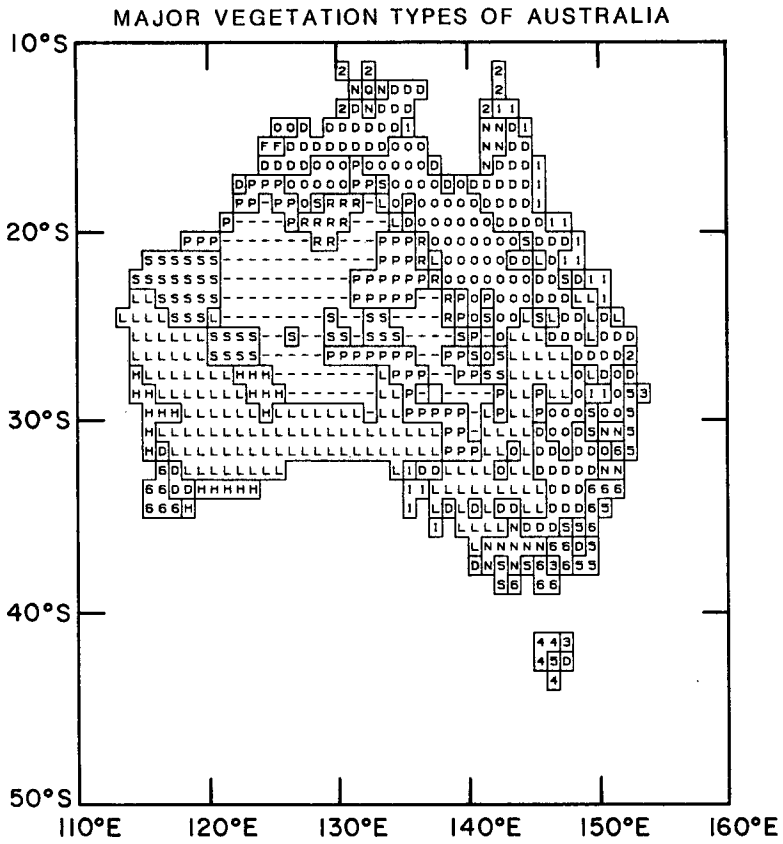

FIG. 6c. Major vegetation types of Australia (Matthews, 1983, 1985). See Table 1 for descriptions and explanation of symbols.

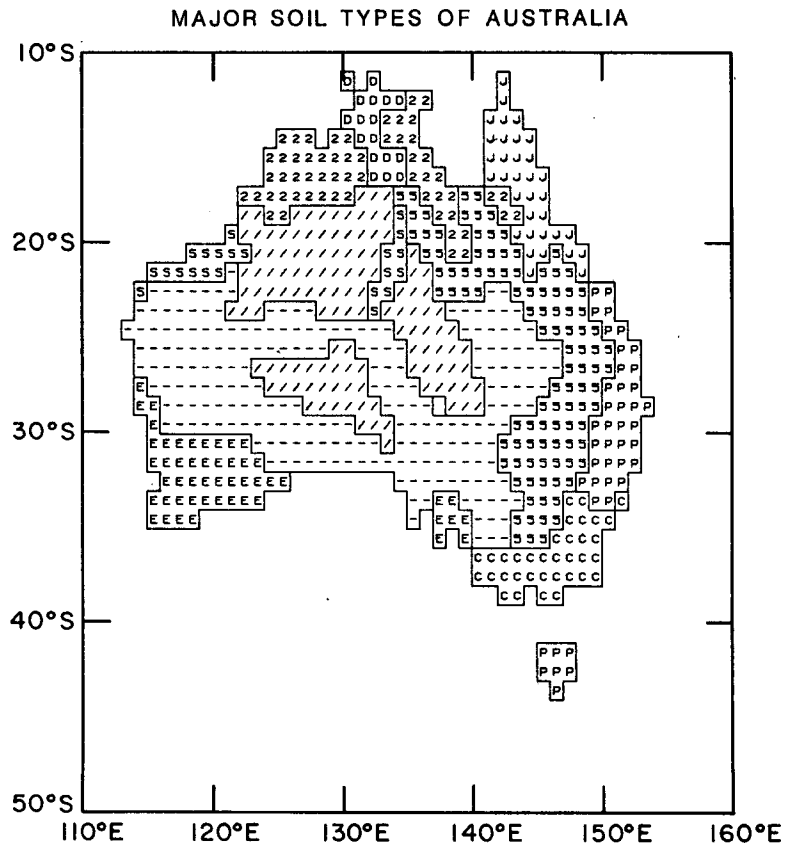

FIG. 6d. Major soil types of Australia (Oxford Atlas, 1973). See Table 2 for descriptions and explanation of symbols.

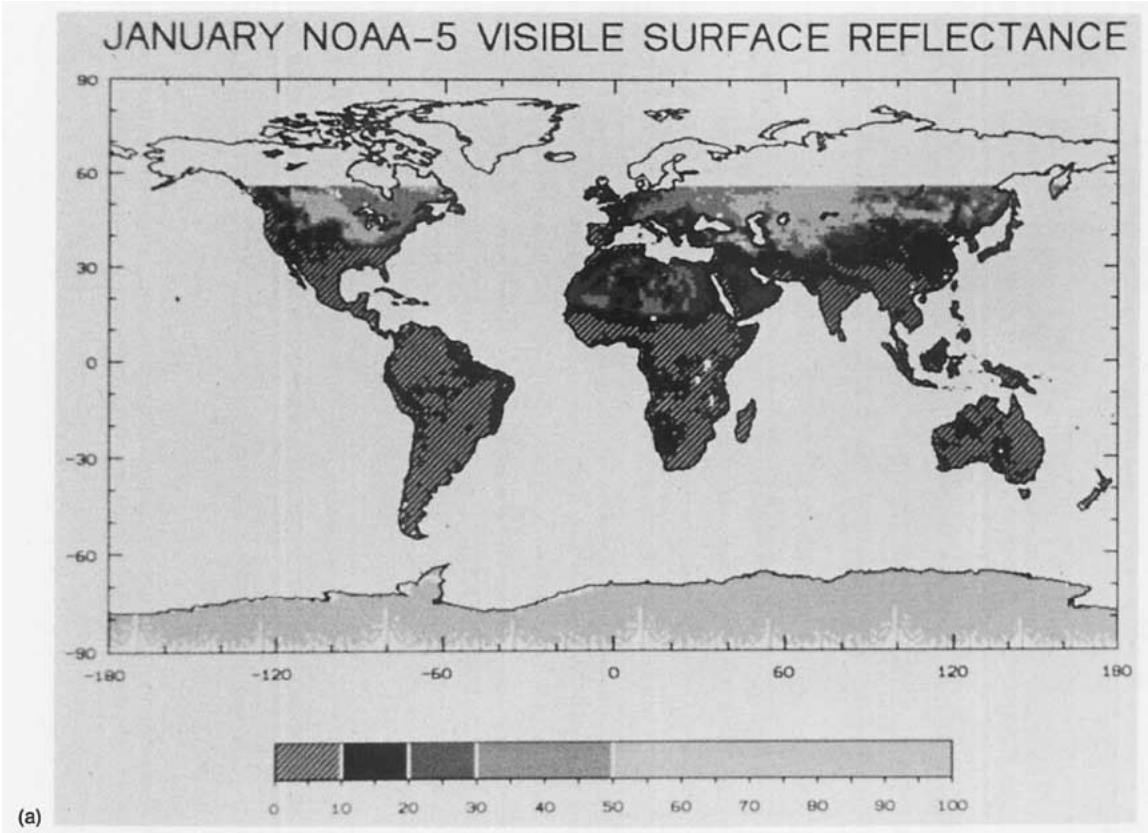

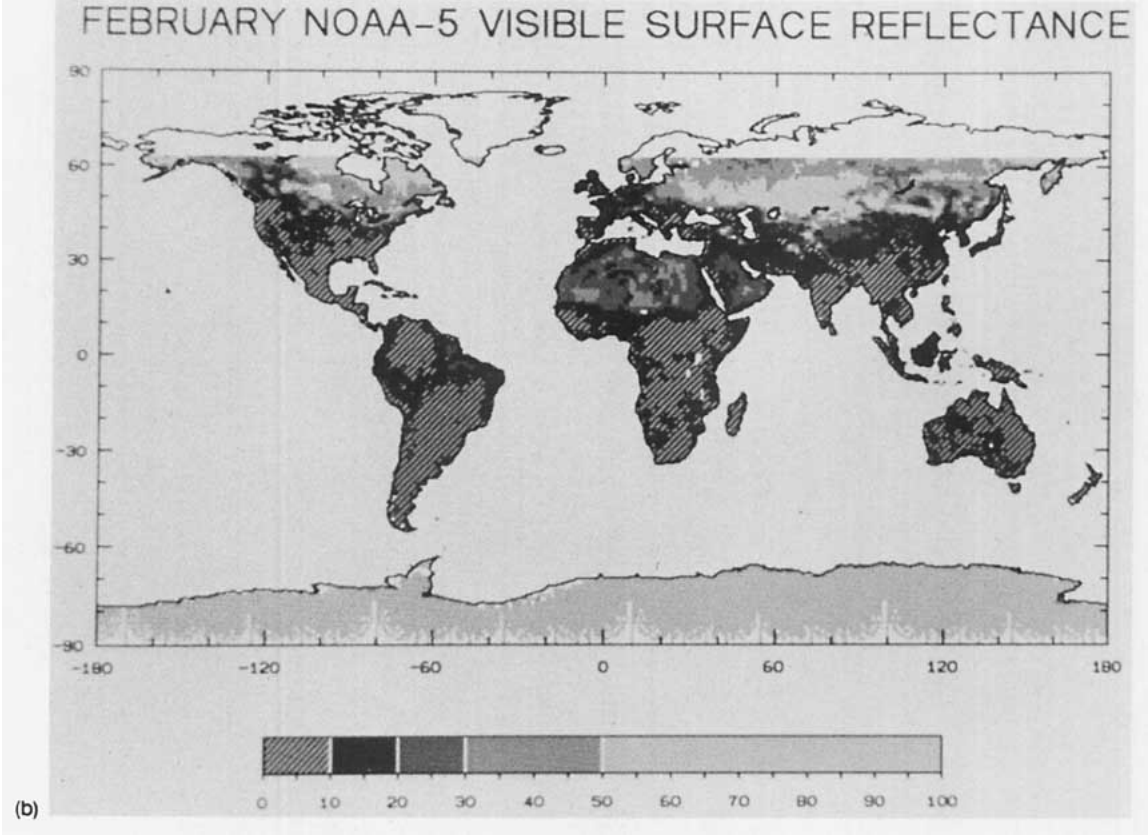

FIG. 7. Global visible surface reflectance for (a) January, (b) February, (c) April, (d) July and (e) October 1977. Patterned areas are <10% reflectance.

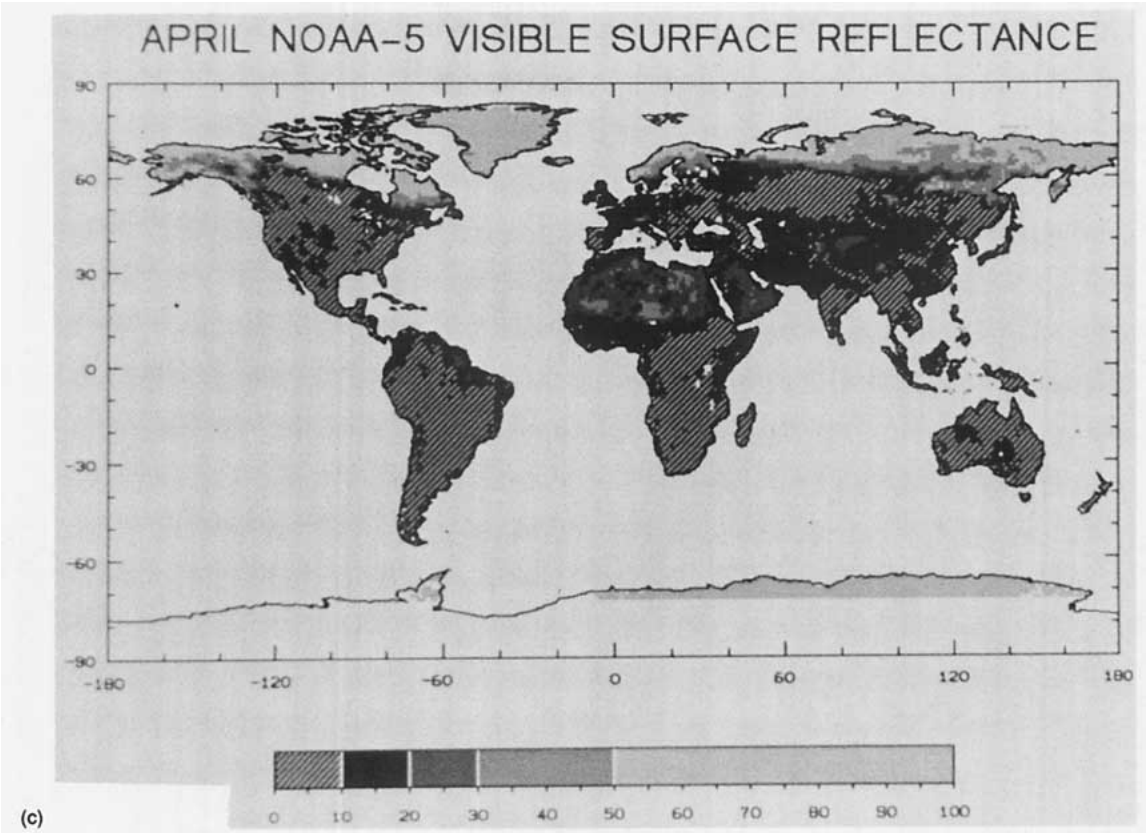

(c)

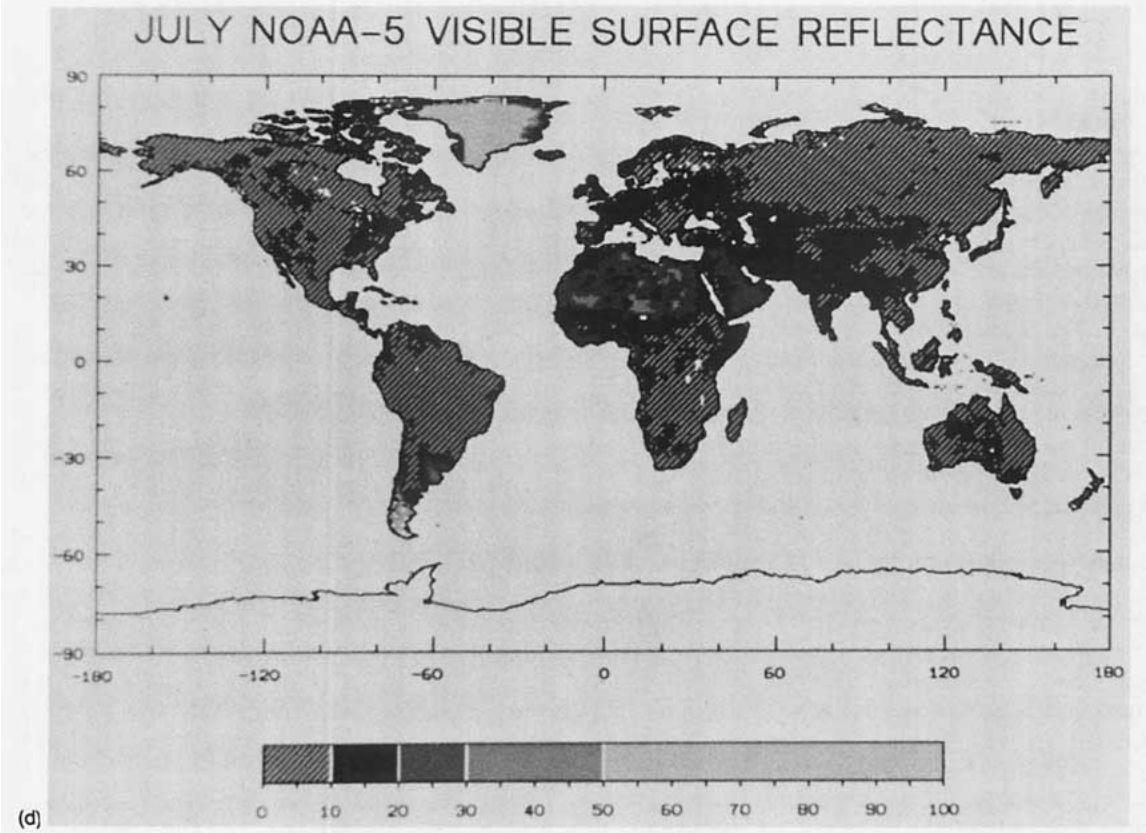

(d)

FIG. 7. (*Continued*)

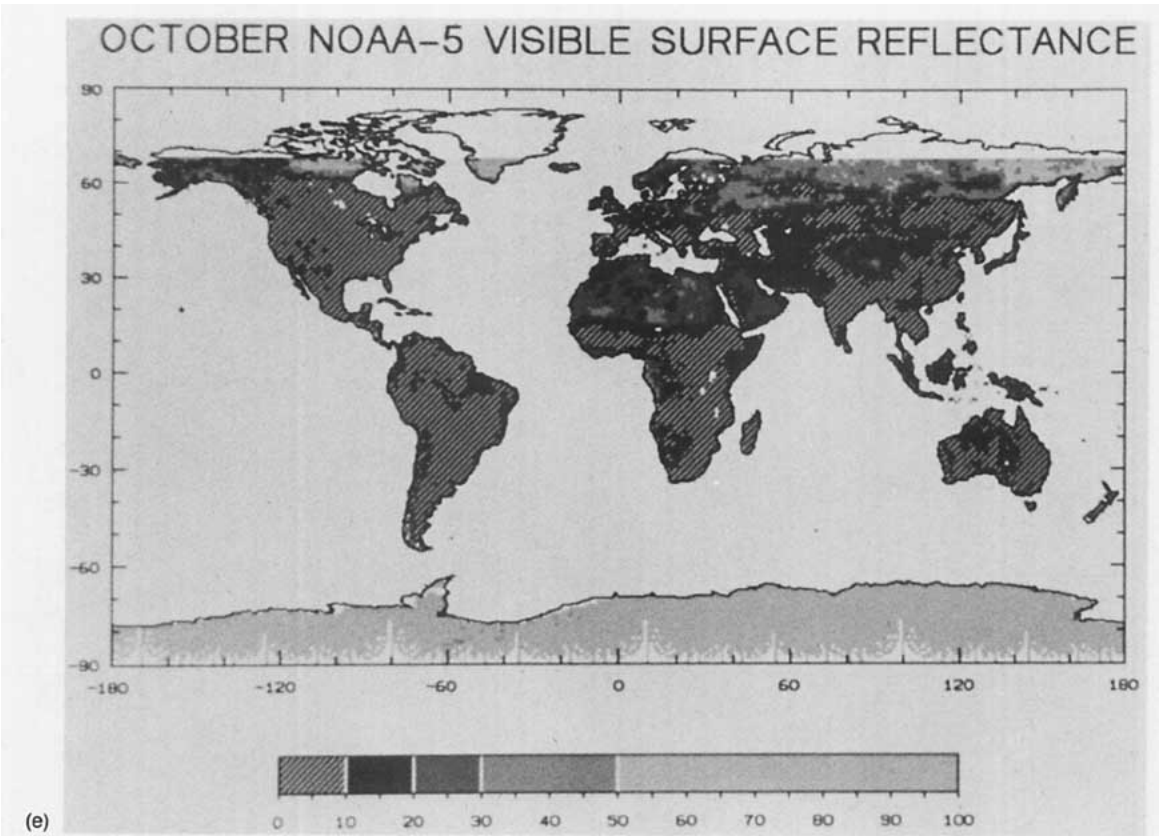

FIG. 7. (*Continued*)

to tundras; short grasslands/cultivated lands of western Asia (between 40°–80°E at about 50°N) produce southward tongues of high reflectance (>50%) during the winter months due to snow cover.

The dark Australian and southern African deserts exhibit reflectances only a few percent brighter than the surrounding arid vegetation types but are clearly delineated here because they are just over 10% in reflectance. The Saharan/Arabian deserts are seasonally stable features with reflectivities generally between 20–30%, punctuated by the bright sand fields of Mauritania (El Djouf), Niger (Tenere) and Libya as well as dark mountains such as the Atlas, Ahaggar and Tibesti. The relatively sharp reflectance gradients southward of 15°N (Fig. 5a, 5b), which coincide with the well-known Sahelian vegetation/aridity gradient from arid shrub grasslands to more humid grassland complexes with tree cover, are smoothed out here. The western coast of tropical Africa exhibits anomalously high reflectance patterns, most pronounced in October, indicative of residual cloud contamination. (Fig. 4a, section 3c).

South America exhibits relatively homogenous reflectance of ≤10% throughout the year except for 1) regions of persistent cloudiness extending from the mouth of the Amazon (see section 3c) and La Plata, 2) arid regions along the eastern coast between 5°–20°S, and 3) southern areas brightened by July snow cover.

These results suggest that only a few simple land types can actually be distinguished by their *visible* reflectance values (see section 6), despite the fact that boundaries between land-cover types with similar reflectance characteristics are realistically and repeatedly reproduced in these reflectance data (e.g., Figs. 5 and 6). In other words, the only land types which are recognizable by 0.6 μm reflectance *alone,* with statistical significance, are forests/woodlands, grasslands, shrublands, deserts and ice.

b. Seasonal snow-free reflectance of land-cover types

Table 3 shows a global comparison of summer and snow-free winter (or wet and dry season where applicable) mode reflectances, along with half-power reflectance ranges[3] for the vegetation types listed in Table 1. For vegetation types that have a winter growing season (e.g., No. 17) or occur only in the Southern Hemisphere (e.g., No. 3, 4), summer (growing season) values

[3] The table shows the relectance values above and below the mode that occur half as frequently as does the mode value.

TABLE 3. Modal values and half-power ranges for vegetation types; summer (rainy season), snow-free winter (dry season), snow-covered winter (dry season).

Vegetation type	Summer†			Winter					
				Snow free#			Snow-covered$		
	No. obs.	Mode	½ Power	No. obs.	Mode	½ Power	No. obs.	Mode	½ Power
1	1025	5	4, 9	1025	9	7, 11	—	—	—
2	321	9	7, 11	320	7	6, 9	—	—	—
3	17 (Ja)	7	6, 8	17 (Jl)	8	7, 11	—	—	—
4	44 (Ja)	6	4, 9	40 (Jl)	9	7, 11	—	—	—
5	93	9	7, 10	92	11	9, 12	—	—	—
6	44	9	8, 11	44	7	6, 11	—	—	—
7	48	7	6, 13	48	5	4, 7	—	—	—
8	1377	7	5, 9	1377 (Ap)	7	6, 11	1085 (Fe)	37	27, 49
9	254	7	6, 11	254	7	6, 9	—	—	—
10	574	9	7, 11	520 (Fe)	7	6, 11	520 (Fe)	45	35, 53
11	513	7	5, 8	226	7	6, 9	475 (Fe)	47	45, 53
12	227	7	5, 9	227	7	5, 8	—	—	—
13	149	7	6, 11	149	7	6, 9	—	—	—
14	360	7	5, 11	159	5	4, 6	159 (Ja)	49	45, 50
15	353	7	6, 8	353	9	8, 10	—	—	—
16	503	5	4, 7	—	—	—	503 (Ap)	49	45, 61
17	—	—	—	122 (Jl)	11	7, 13	—	—	—
18	90	5	4, 9	76 (Fe)	9	7, 13	76 (Fe)	—‡	—‡
19	77	11	9, 12	77	9	8, 13	—	—	—
20	94	9	7, 10	—	—	—	94 (Ap)	65	63, 69
21	868	9	8, 13	871	9	7, 11	871 (Ja)	59	51, 63
22	1460	7	5, 9	—	—	—	1462 (Ap)	72	67, 75
23	611	7	5, 8	606	7	6, 11	—	—	—
24	347	9	8, 11	332	9	7, 10	—	—	—
25	911	9	7, 13	911	9	8, 13	—	—	—
26	72	9	8, 10	72	7	6, 9	—	—	—
27	72	9	7, 11	72	9	7, 11	—	—	—
28	604	9	7, 11	606	9	9, 11	606 (Ja)	53	49, 55
29	49	5	4, 7	—	—	—	—	—	—
30	1549	23	3, 27	1367	21	11, 31	1555 (Ap)	69	65, 75
31	764*	73	71, 75	—	—	—	5723 (Ja)*	85	79, 87

* Summer values for Greenland; winter values for Antarctica.
† Summer values are for July unless otherwise indicated in parentheses.
# Snow-free winter values are for January unless otherwise indicated in parentheses.
$ Snow-covered winter values are for months indicated in parentheses.
‡ No clear mode is apparent; snow-covered points are variably dispersed throughout the range from 60–74%.

are from January and winter values are from July. Because of winter illumination conditions, winter values may be from January, February or April in the Northern Hemisphere, and from July or October in the Southern Hemisphere. As suggested in section 2c, summer/wet season values are generally equal to or a few percent lower than snow-free winter values. Forests (No. 1–13) and woodlands (No. 14–16) generally exhibit lower reflectances, while more arid and lower-statured grasslands (No. 23–28) and shrublands (No. 18–21) show higher reflectances. Several forest types (Nos. 1, 2, 5) occupy some regions that are subject to persistent cloudiness. Tundras (No. 22) and arctic meadows (No. 29) are relatively dark, perhaps due to waterlogging during the thaw season. In cases where summer and winter modes are the same, some though not all vegetation types show narrower reflectance distributions in summer. Desert (No. 30) modes (21 and 23% for the two seasons) are dominated by the relatively bright Sahara but the distributions are broad and seasonally stable; seasonal variation in this case is probably dominated by the solar zenith angle dependence of the surface reflectance.

The previous discussion of seasonal variations of surface reflectance combines solar zenith angle dependence with intrinsic surface property variations with season. These two effects may contribute differently to the total effect, but they cannot easily be separated from an analysis of polar orbiter data alone. Use of geosynchronous satellite observations to isolate solar zenith angle effects may help in making this separation.

c. Global and regional homogeneity of land-cover types

In subsection 5b, we briefly outlined summer and winter reflectance ranges for global distributions of

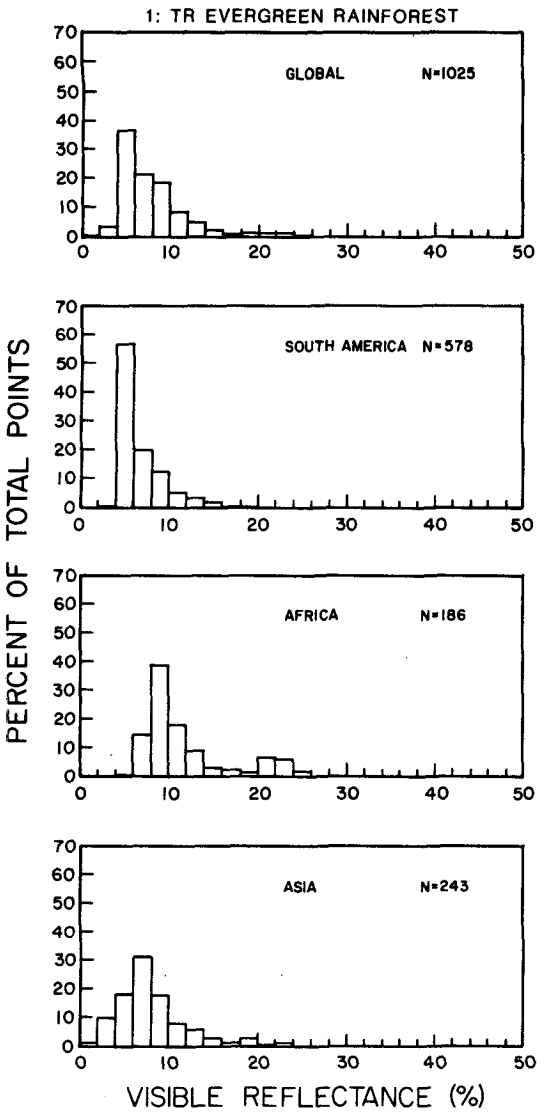

FIG. 8. July reflectance histograms for global and continental distributions of No. 1 tropical evergreen rainforest (see Table 1).

land-cover types. In the following, we expand the analysis of the summer values in order to evaluate and explain regional variations.

Tropical rainforests are often located in regions of persistent cloud cover (section 3c), the effects of which are most prominent in Africa in July and October, and in South America in February. July reflectance histograms for global and continental distributions of tropical rainforests (No. 1 in Table 1) are shown in Fig. 8. The global distribution exhibits a mode value of 5%, with an additional 40% of the points between 6–10%. South America displays a stronger 5% mode; the drier Asian formation peaks at 7%, with trailing brighter values indicating cloud contamination. For the driest African distributions, the mode value is 9% with higher values trailing into the mid-20s, but the cloud-free April mode for African rain forests is 7% (Fig. 4b).

Temperate/subpolar, evergreen, needleleaved forests (No. 8) are distributed equally among North America (two distinct formations), Europe and Asia. The reflectance histogram for global distributions (Fig. 9) shows a wide spread from 4–12%. The North American points are similarly widely dispersed (including the overlapping distributions of the two formations), while the European points are clustered in the higher range and the Asian points in the lower range. Since latitude ranges (and therefore solar zenith angle, ozone etc.) are similar for the European and Asian forests, a possible explanation is that the status of the forests themselves differ between the two continents, with the

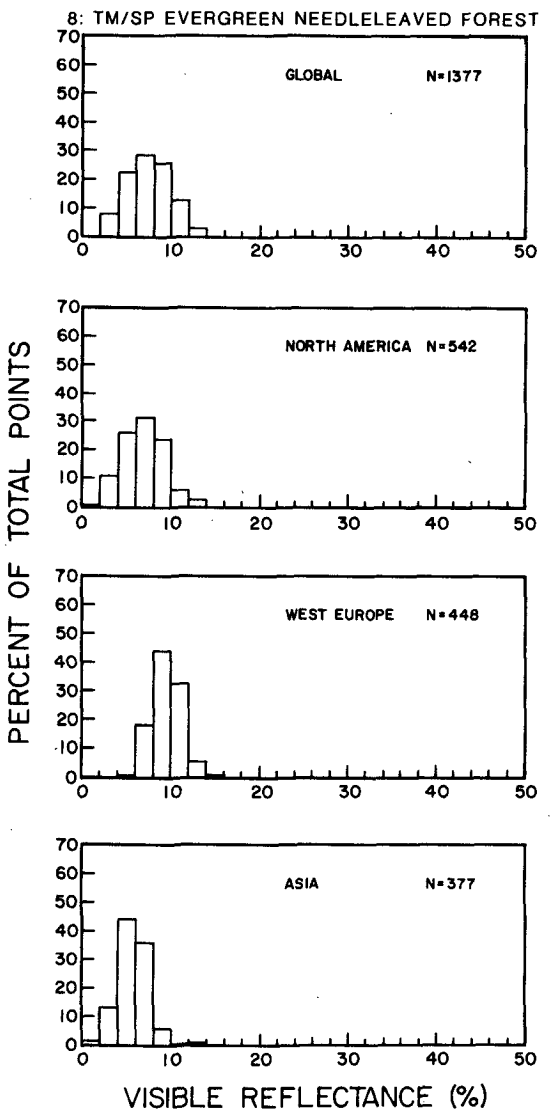

FIG. 9. As in Fig. 8 except for No. 8 temperate/subpolar evergreen needleleaved forest.

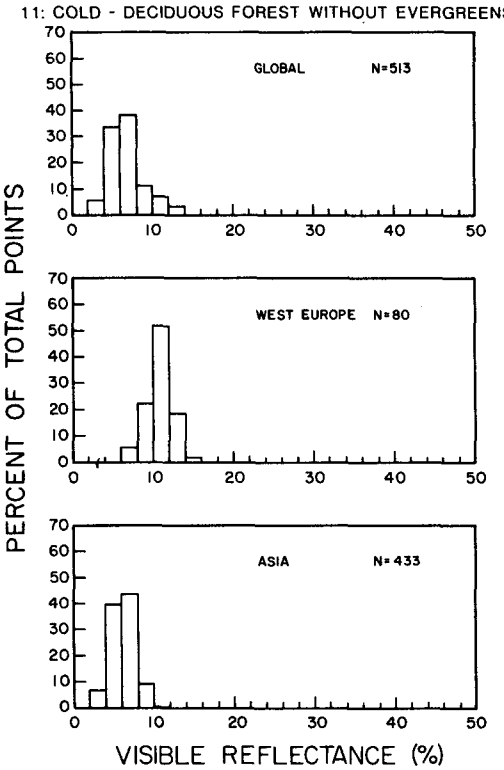

FIG. 10. As in Fig. 8 except for No. 11 cold-deciduous forest without evergreens.

Asian formation perhaps more vigorous or dense. A majority of the European points are located in mountainous terrain, which not only can modify the local structure of the vegetation but also can introduce larger variations in retrieved reflectance values related to viewing geometry. Similar continental distinctions are apparent in the histograms for cold-deciduous forests with evergreens (No. 10) and in cold-deciduous forests without evergreens (No. 11; shown in Fig. 10). In these cases, the European locations have probably been subjected to greater anthropogenic disturbance, resulting in reduced density.

Seasonal, tropical/subtropical, drought-deciduous forests (No. 9) occur in India and east-central South America. Figure 11 shows global and continental reflectance histograms for this cover type for October as well as July. The July values for Asia appear to be anomalous, probably due to persistent summer monsoon cloudiness over India. For both continental locations, reflectance minima in the range of 6–10% occur in October coinciding with rainfall maxima and vegetative development. The July–October distributions for Asia suggest either that this type is very heterogeneous during the nonfoliated dry period (July) or that the July data are contaminated with clouds. The South American mode is the same for the two months, although the overall distribution shifts slightly higher in July. The Asian component shifts substantially in mode and overall distribution, with virtually all points $\leq 10\%$ in October and $>10\%$ in July.

July reflectance distributions for a series of woodlands (Nos. 14, 15, 16) are shown in Fig. 12. Evergreen needleleaved woodlands (No. 14) occur almost exclusively in high latitude North America; drought-deciduous woodlands (No. 15) are concentrated in subtropical Africa; and cold-deciduous woodlands (No. 16) are found in Asia, northward of 70°N. Evergreen needleleaved woodlands (No. 14), if occurring on homogenous terrain, would be expected to display low and relatively restricted reflectance ranges. A plausible explanation for the wide dispersion from 2 to 12% is the occurrence of these forests in mountainous locations in northwest and southeast Canada. As just sug-

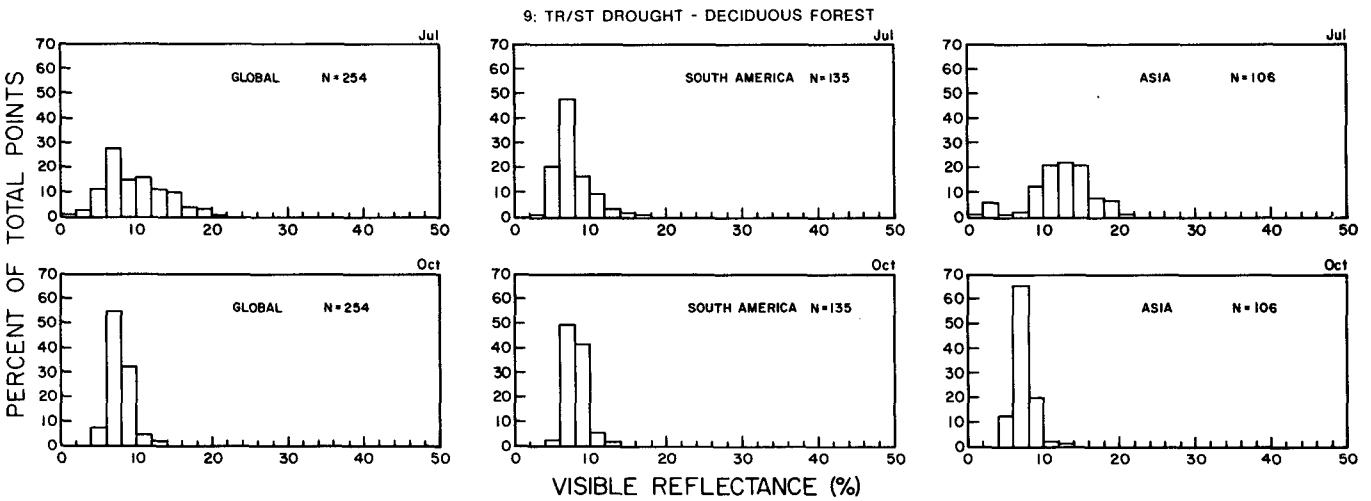

FIG. 11. July and October reflectance histograms for global and continental distributions of No. 9 tropical/subtropical drought-deciduous forest (see Table 1).

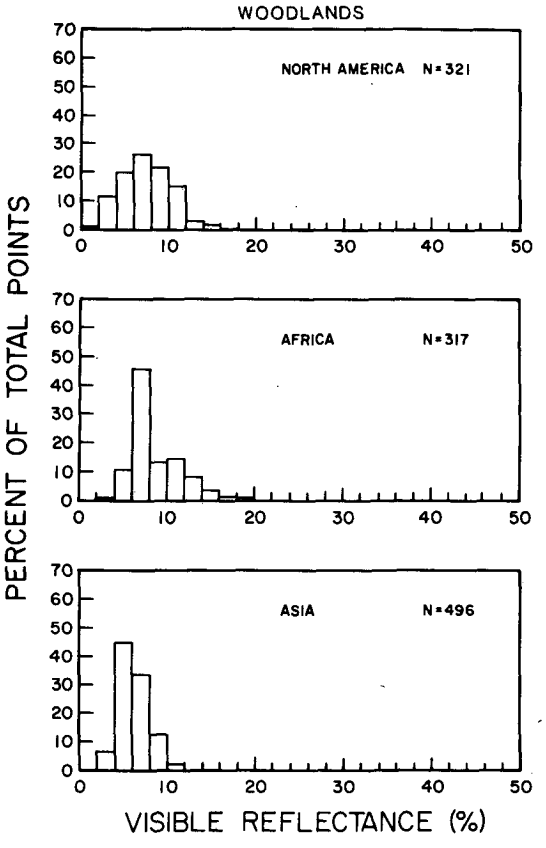

FIG. 12. July reflectance histograms for three woodlands. Each of these types is restricted almost exclusively to one continent; only the characteristic continent's distribution is shown: North America, No. 14 evergreen needleleaved woodland (top panel); Africa, No. 15 drought-deciduous woodland (middle panel); Asia, No. 16 cold-deciduous woodland (bottom panel).

gested, such topographical factors can introduce variability into both local stand structure and the geometry of satellite observations. Arid and spatially variable drought-deciduous woodlands (No. 15) expectedly display a wide (yearlong) reflectance dispersion although they exhibit a low mode of 7%. The seasonally stable distribution suggests that while drought-deciduous woodlands are generally of low reflectance, spatial inhomogeneities within the ecosystem produce consistent reflectance limits of 4–14%. Asian cold-deciduous woodlands (No. 16) exhibit a low and restricted reflectance range, with 80% of the points clustered between 4–8%. The classification of this type is, however, more precise and the geographic location more restricted than for most ecosystems, which may explain its more homogeneous appearance.

The grassland formation, composed of wooded and nonwooded subgroups with varying tree heights and densities, occupies a dispersed area equal to about 20% of the ice-free land surface of the earth. One of the more humid groups, grassland with 10–40% tree cover (No. 23), occurs in a series of environmental regimes: in equatorial South America and Africa, this formation rings the southeastern perimeter of tropical rainforests; in Asia it is found as a transition between shrubbed or short grasslands and cold-deciduous forests. More arid distributions are found in Sahelian Africa dispersed among several arid grasslands, and in Asia between deserts and xeromorphic shrublands. With increasing aridity, grass cover decreases and shrubs replace trees as the woody component of grasslands. Arid grasslands with shrub cover (No. 25) are widely distributed, with major concentrations at the southern Saharan border in North Africa and between xeromorphic woodlands east of the Gobi and cold-deciduous forests extending to the Pacific Coast of eastern Asia. The global July reflectance histogram for the humid grasslands (No. 23) shows a wide dispersion from 4–14%, with some points ranging to 20% (Fig. 13). The South American and Asian formations contribute to the lower restricted range between 4–8%, while the African plot exhibits the breadth expected from the combination of the arid (Sahelian) and humid (equatorial) components of this formation. In addition, some of these African points are within the July cloud contamination area (Fig. 4a). Figure 14 shows the July distributions of the arid and variable grassland with shrub cover (No. 25). The global plot shows a wide reflectance distribution, clearly brighter than that indicated for forests, woodlands and grasslands with tree cover, with most points concentrated in the range of 8–14%. The histogram structure of the African distributions is consistently (seasonally) different from the other continents. When the reflectances of Northern and Southern Hemisphere points are analyzed separately, however, this shrub/grassland type shows a high mean (14–16%, ±6% each month) in the Saharan north and lower values (monthly means of 7–9%, ±2%) in the more humid Southern Hemisphere. This suggests the possibility either that the classification is not precise enough to distinguish regional variations or that the classifications in northern Africa might be in error due to the persistent drought in this region (C. J. Tucker, personal communication, 1985). Both the Asian and Australian formations are more homogeneous and darker than the African type in their reflectance behavior (see section 4c).

Arid environments, i.e., desert and xeromorphic shrubland, woodland and forest, occupy almost one-quarter of the ice-free land surface of the earth; their important role in climate was recognized early (Charney, 1975; Charney et al., 1977; Sud and Fennessy, 1982). These cover types are expected to be bright, seasonally stable and subject to high insolation due to persistent cloud-free conditions and low-latitude locations. Deserts, occupying ~12% of the global ice-free area, are restricted almost exclusively to subtropical subsidence zones in both hemispheres, with a few scattered polar deserts in northern Canada. Because vegetation is essentially absent and a wide variety of soil and rock materials govern desert reflectance, we find

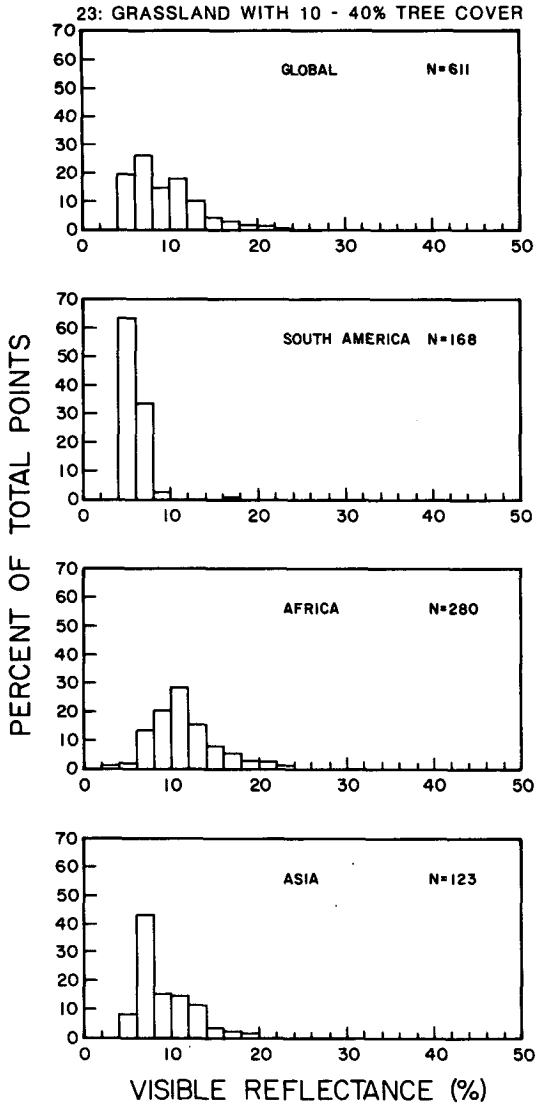

FIG. 13. As in Fig. 8 except for No. 23 grassland with 10–40% tree cover.

significant spatial variation but relatively stable temporal behavior in the reflectance properties of deserts. Intercontinental comparisons of July desert reflectance distributions are shown in Fig. 15. The main feature of these histograms is the wide variety of reflectance values exhibited. The darkest are the Australian deserts, with a mean of 11 ± 2% in July. The dominant soils in these regions are shallow psamments (sandy soils) and undifferentiated aridisols (Nos. 3 and 11 in Table 2). Since color is not a classification criterion in soils classification systems, it is not surprising that reflectance histograms for deserts are not consistently explained in terms of soil classes although some geographic reflectance patterns in Australia and Asia do correlate with soils (section 4c, Fig. 6). North American deserts in Canadian polar areas are clustered between 14–16%. About 40% of the points are associated with seasonally wet polar inceptisols (No. 7) which are dark in color; the remainder are made up of entisols and cryic great groups of variable color. Asian deserts exhibit a broader, flatter reflectance distribution than the preceding two, with a July mean of 12 ±4.5%. About 20% of the points, in polar locations, are associated with dark, seasonally wet inceptisols (No. 7). The southern Gobi is composed of general cryic great groups, while the northern sector has brighter aridisols (No. 11). These Asian latitudinal gradations appear in the monthly reflectance maps but are obscured in the histograms. African and Arabian deserts, which dominate the brighter range of the global histogram, are broadly distributed between 20–30% (mean = 22 ±4.5%). They are located overwhelmingly on light-colored aridisols (No. 11) and secondarily on sandy

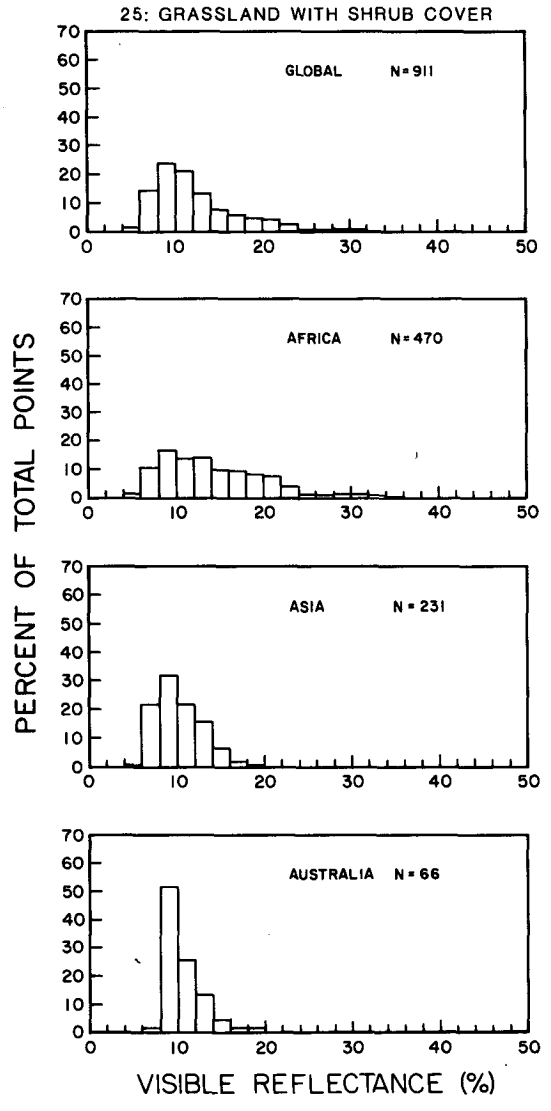

FIG. 14. As in Fig. 8 except for No. 25 grassland with shrub cover.

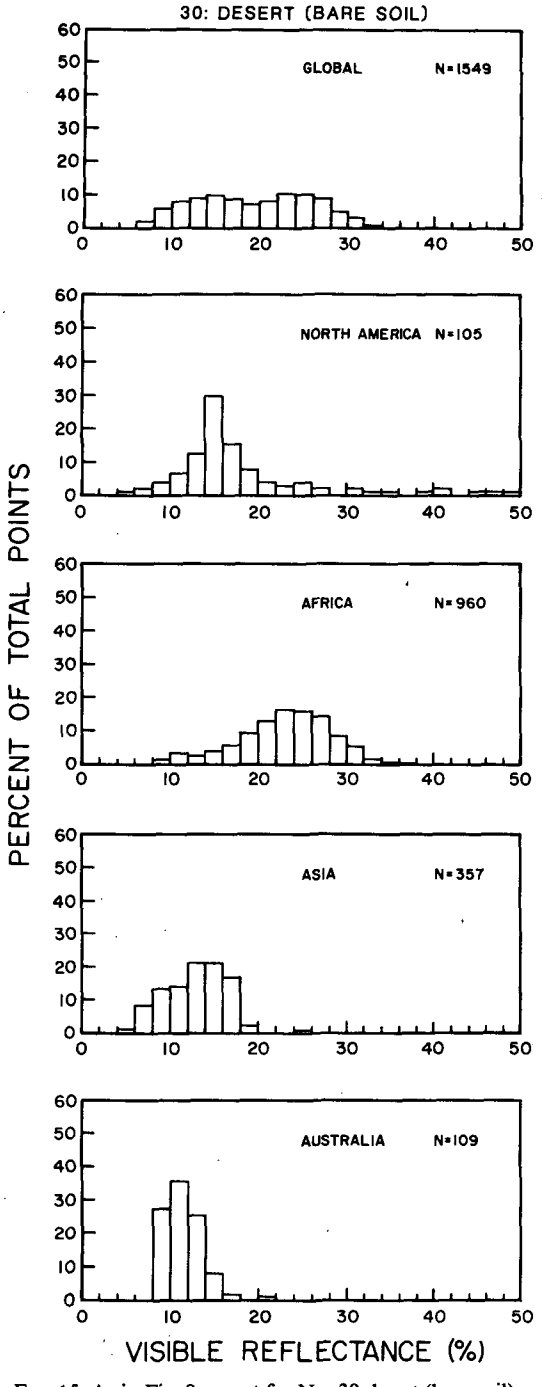

FIG. 15. As in Fig. 8 except for No. 30 desert (bare soil).

psamments (No. 3), and are the only deserts associated with soil classes of consistent color. As a group, deserts show expected wide variations and seasonally stable behavior as found by Staylor and Shuttles (1986). Although African deserts exhibit reflectances ~5–10% lower than those prescribed in climate models, Asian, Australian and North American deserts are considerably darker, bridging the gap between vegetation reflectances (<10%) and expected desert reflectivities (>25%).

Xeromorphic shrublands, accounting for ~8% of the ice-free land surface, are distributed in subtropical and temperate regions along desert perimeters and in montane rainshadows. The greatest extent of this ecosystem occurs in Africa, with additional distributions in South America, Asia and Australia, and smaller extents in North America and Western Europe. Figure 16 shows July reflectance histograms for distributions of xeromorphic shrublands (No. 21). The global composite exhibits an unexpectedly low mode of 9% with the remaining points trailing upward to 22%. However, continental distributions show clearer patterns. The South American and African histograms are similar to the global case. (Some of the South American shrublands are snow covered in July.) However, the northern and southern portions of African xeromorphic shrublands are distinct, with higher ranges in the Saharan and Sahelian north (mean of 13–15 ± ~6% in every month) and lower ranges in the south (monthly means of 8–9 ± 1–2%), similar to the regional distinctions found for shrub/grasslands (No. 25) discussed previously. Dry shrublands in Asia display a broad, bright distribution similar to that of Asian deserts. The Australian group is darker and shows a more marked mode as is the case for Australian deserts. Dominant soils underlying xeromorphic shrublands on all continents are primarily undifferentiated aridisols (No. 11 in Table 2), with contributions from ustolls (No. 17), ustalfs (No. 25) and xeralfs (No. 26). However, xeromorphic shrubland is not a precisely defined cover type, and therefore includes spatially heterogeneous components; underlying soils are not well defined in regard to color. Therefore, reflectance histograms display local variability that is difficult to interpret.

The arid cover types discussed here generally show brighter and more dispersed reflectance distributions than those of forests, woodlands and grasslands consistent with expectations; spatial heterogeneity is also much greater in these cover types. In addition, both continental and hemispheric reflectance variations are ecologically reasonable.

Tundras are restricted primarily to locations north of 60°N, with scattered distributions in lower latitude alpine areas. In western North America, the tundra–forest boundary extends along 70°N before dropping 1500 km southward to encircle Hudson Bay; this boundary can be seen in the reflectance maps at 3–5% contrast but becomes more distinct with snow cover (Robinson and Kukla, 1985). European and Asian tundras are more restricted to areas north of 70°N, except in eastern Soviet Union. The global distribution of tundras is concentrated in the range from 4–12% (Fig. 17). There is some suggestion that the Asian variety, strongly clustered between 4–8%, may be slightly darker and more homogenous. Most North American and European distributions are either alpine or made

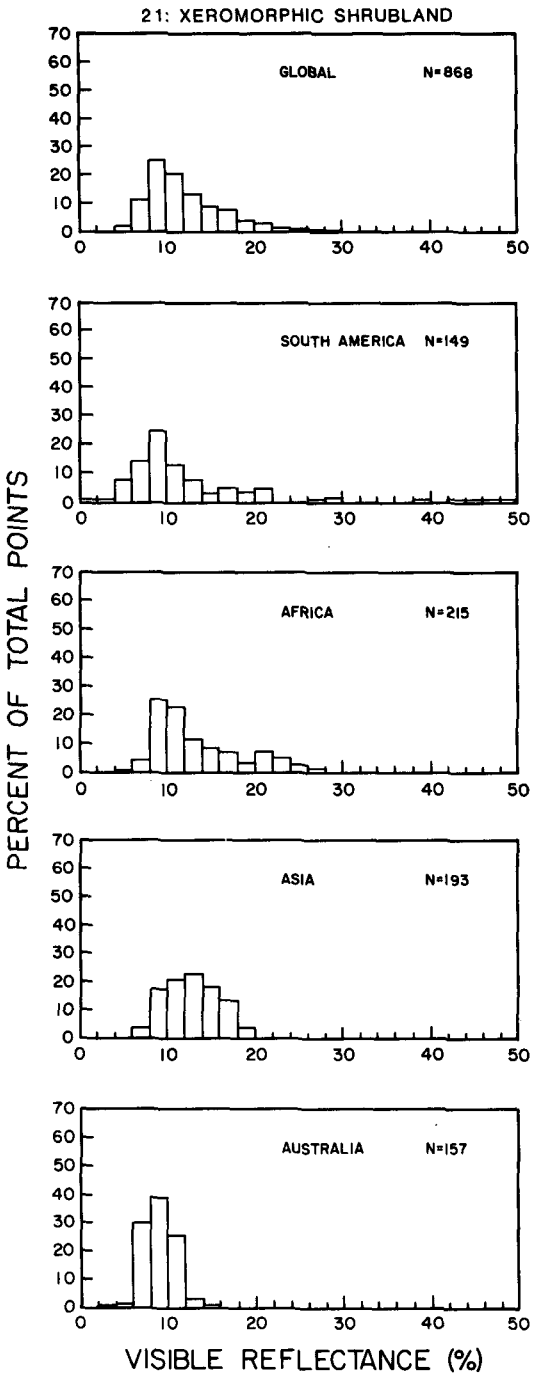

FIG. 16. As in Fig. 8 except for No. 21 xeromorphic shrubland.

up of dwarf shrub and lichen complexes, both of which may be expected to be lighter colored and therefore brighter. Mossy bogs southwest of Hudson Bay are represented in the lower ranges for North America.

d. Snow brightening for cover types

The variable increase in surface albedo produced by a given depth of snowfall over different vegetation types is related to vegetation height and density. The magnitude of snow brightening effects was investigated with these NOAA-5 data using the same histogramming technique discussed above for snow-free vegetation. Table 3 shows mode and half-power reflectance values for snow-free and snow-covered winter conditions for a series of vegetation types. No attempt is made at this stage to remove solar zenith angle dependence.

Since forests and woodlands are taller and denser than the remaining cover types and therefore mask snow more efficiently, visible reflectances for snowy conditions in forests and woodlands are lower than those for shrublands, deserts and tundras. Temperate/subpolar evergreen needleleaved forests (No. 8), with high year-round canopy closure and dark color, still show a five-fold increase in mode reflectance between

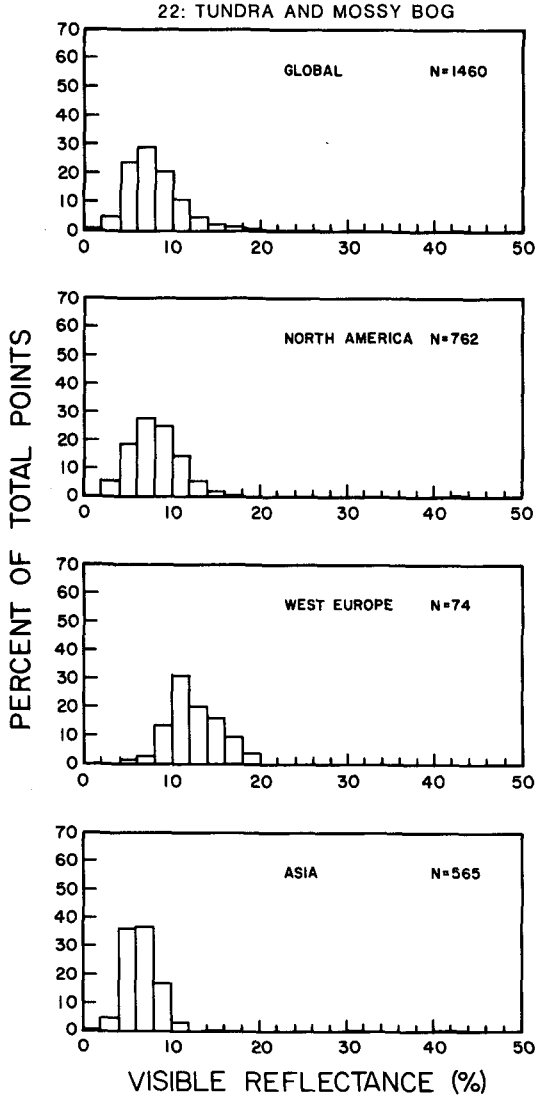

FIG. 17. As in Fig. 8 except for No. 22 arctic/alpine tundra and mossy bog.

July and February (snowy) conditions. The wide range for snow brightening (+12 and −10% around the mode of 37%) is three–five times larger than for snow-free conditions and reflects latitudinal ranges (temperate to boreal) and associated ecosystem variations of the canopy structure of this type. Evergreen needleleaved woodlands (No. 14), a sparser and more boreal version of the evergreen needleleaved forests, exhibit a mode about 10% brighter than that for the forests. The narrow range about the mode may be explained by the fact that this type is geographically much more restricted. Several deciduous forests (Nos. 10 and 11) display mode values brighter than evergreen forests and darker than woodlands and low-stature cover types. While both of these forests have the same upper half-power values and similar modes, deciduous forests with evergreens (No. 10) can be considerably darker under snowy conditions. Shrublands (Nos. 18 and 20), which are low in height and density, show snow reflectances from 63–74%, while very low statured tundras (No. 22) range from about 65–75%. Two desert regions are seasonally snow-covered (Asia and North America). They display generally similar summer and winter values, with the snow-covered winter values coinciding with the upper ranges for snow-covered shrublands and tundras (~65–75%). Low illumination levels, in conjunction with long atmospheric path lengths (ozone corrections alone are on the order of 10–15% in these high-latitude locations), suggest the need for caution in interpreting visible reflectances for permanently snow-covered land ice; however, these results show a mode reflectance for Antarctica (No. 31, snow-covered winter) that is about 10% brighter than that for Greenland (No. 31, summer).

6. Summary and conclusions

We have presented a set of global, seasonal, *visible* surface reflectance maps derived from NOAA-5 Scanning Radiometer observations. The internal consistency and statistics of these results, as well as their comparison to other data, have demonstrated the feasibility of obtaining an accurate global survey and of monitoring of surface *albedo* from satellites, and provided a preliminary assessment of variations of visible surface reflectance, especially that caused by snow cover.

a. Methodology

Because of the number of atmospheric and surface factors which contribute to variations in the radiances measured by a satellite for a given location, analysis methods that depend on retrievals of a single value (e.g., the minimum) are less accurate than statistical approaches. Although rather simple techniques can be used to identify clear-sky observations for most regions, some areas of persistent cloudiness or rapid surface variations require more careful study to obtain accurate results. These areas on land are 1) several areas of tropical western Africa, Amazon Basin, Indonesia and Southeast Asia; 2) snow-cover boundary zones (approximately ±200 km on either side of the monthly mean position) that undergo rapid snow-cover variations; and 3) polar regions. We have found that reliable satellite measurements of surface properties in some tropical regions can only be accomplished in certain seasons, whereas the snow boundary problem is confined to certain "active" regions and seasons. The polar regions are generally difficult because of the low (or reversed) radiance contrast between cloudy and clear scenes, although some evidence suggests persistent cloudiness may be a problem in some seasons (Herman and Goody, 1976; Crane and Barry, 1984).

The consistency of some surface reflectance patterns over time, even those produced by reflectance contrasts as small as ~3%, suggests that our statistical approach obtains accurate enough values for each location to allow meaningful measurements of seasonal, geographic and ecosystem variations of different land types utilizing land-cover and soils data bases. Our results also show that the variability of *visible* reflectances is relatively small, ~5–10%, requiring high accuracy for its study. Smaller time and space variations require higher time/space resolution data sets, however, than obtainable from polar orbiters. Analysis of multisatellite data sets can probably provide a much more detailed global survey as discussed below.

Since removal of cloud contamination is the crucial first step in any analysis of surface properties, the statistics obtained in our study illustrate the value of narrowband observations at ≈0.6 μm wavelength to surface observations. The narrow reflectance distributions exhibited by various surface types demonstrate that variations in atmospheric aerosols, viewing geometry, and vegetation structure produce only relatively small, quasi-random variations in radiances measured at this wavelength, while clouds produce much larger variations. Consequently, this channel provides a strict test for cloudiness (in snow-free conditions) and is useful to surface studies, even though it is not very sensitive to differences in surface properties per se.

However, some atmospheric effects at this wavelength are systematic and must be removed if quantitative comparisons are to be made. For the darker surfaces at lower latitudes, Rayleigh scattering can contribute a significant portion of the satellite measured radiance (the reflectivity of a black surface would appear to be ~6% because of Rayleigh scattering). While monitoring of surface reflectance without correction could be accomplished by maintaining constant viewing geometry, determining the angular dependence of surface reflectance to obtain albedo is difficult without correcting for Rayleigh scattering, especially since the spectral dependence of Rayleigh scattering is so strong. For high-latitude surfaces, the coincidence of large solar zenith angles and ozone abundances produces significant decreases in satellite-observed radiances, opposing

the larger Rayleigh scattering effect. Consequently, a proper determination of the magnitude of the snow albedo feedback from satellite data is difficult without correcting for these factors.

b. *Land cover types*

The relative insensitivity of the 0.6 μm snow-free reflectance measurements to changes in vegetation type (discussed above) limits classification of land surfaces using this wavelength to five basic types: forest/woodland, grassland, shrubland, unvegetated (desert) and ice. The additional use of measurements under snowy conditions could provide more discrimination, however. Figure 18 illustrates this result by showing the proportional contribution of each vegetation class to each 2% reflectance bin. Even though the five groups are evident in such a global summary, the larger variability of the shrub–grassland and unvegetated categories produces overlap with the forest/woodland class; i.e., visible surface reflectance values provide some discrimination among these five groups, but not for all

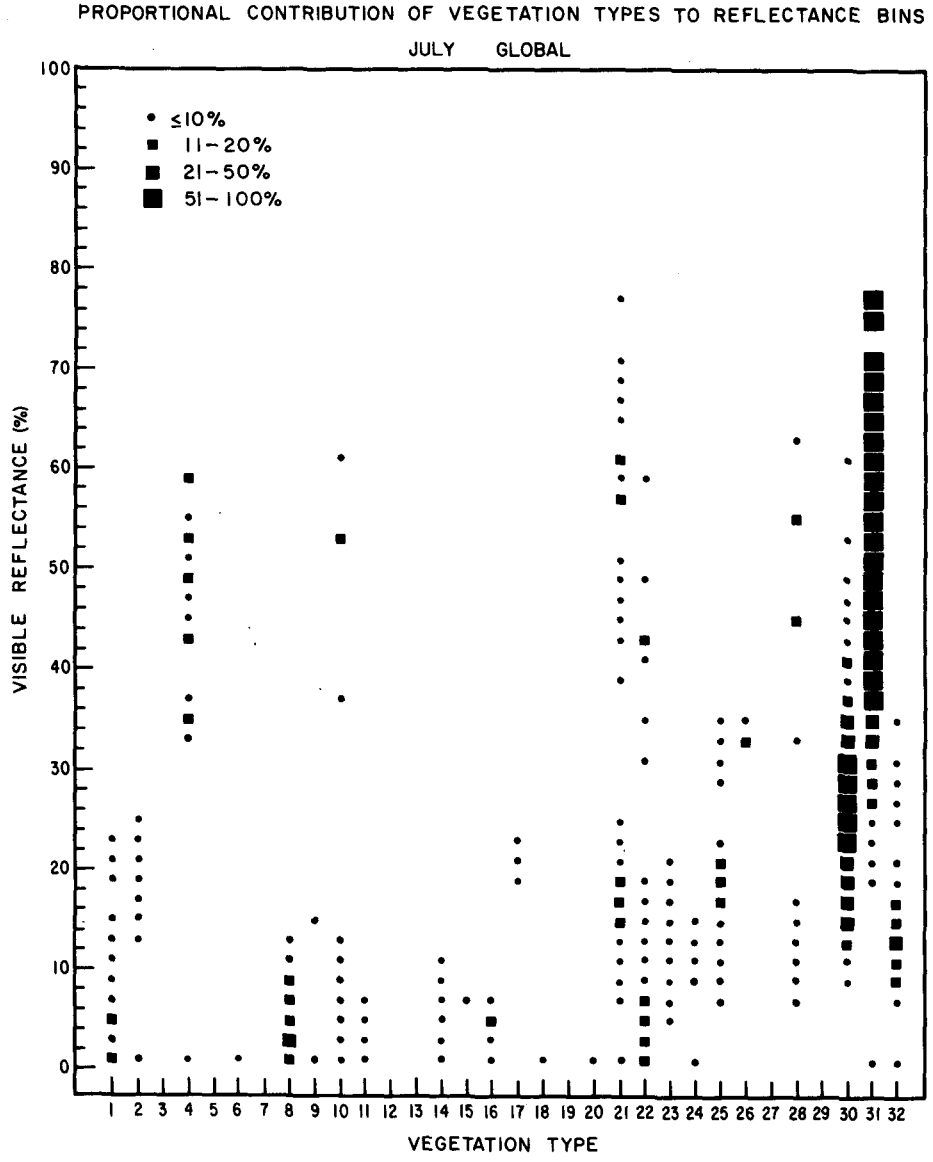

FIG. 18. Proportional contribution of vegetation types to each 2% reflectance bin (July), e.g., 11–20% of all points from 0–2% reflectance are No. 1 tropical evergreen rainforests. Forests and woodlands (No. 1–16) along with tundras (No. 22) are represented in the low reflectance groups (<10%). Concentrations of the more humid grasslands (Nos. 23, 24 and 28) are found from 5–15%, xeromorphic shrublands and shrub/grasslands (No. 21, 25) from 10–25%, nonvegetated deserts (No. 30) from 15–40% and ice (No. 31) above 35%. Note that several cover types (Nos. 4, 10, 21, and 28) are snow covered in July either because of their Southern Hemisphere or high latitude Northern Hemisphere location.

cases. However, when specific geographic locations are considered (e.g., Africa, Fig. 5), large-scale transitions between these groups are generally associated with the appropriate variation of visible surface reflectance. Even though the general correspondence between the land-cover distributions and the reflectance distributions provides some verification of the land-cover data base used here, detailed differences suggest that satellite surveys, compared with surface site checks, should eventually be used to improve the accuracy of spatial distribution in land surface classifications. Use of other more sensitive spectral channels to discriminate among more vegetation classes will be necessary, but our results demonstrate the possibilities of this approach (see also, Tucker et al., 1985; Justice et al., 1985).

The particular land types that are distinguished by 0.6 μm reflectance suggest that the primary factor controlling surface reflectance at this wavelength is the density of vegetation cover. In other words, vegetation appears to be generally darker than most soils, providing a spectrum of reflectances from dense coverage (forests) to sparse coverage (shrub/grassland) to uncovered (desert). Note that this distinction is not very clear for some regions, such as Australia and central Asia, where soils are not much brighter than vegetation. This interpretation also explains the general increase in type heterogeneity with increasing relectance: forests exhibit less variation of reflectance locally or among ecosystems than do shrub/grasslands. Differences in reflectances for similar land types on different continents may also be attributable to differences in density. This diversity of reflectance values within each land-cover class, even for a relatively insensitive spectral region, suggests that specification of surface albedos in climate models with sufficient accuracy to determine proper regional climates (i.e., within 2%) may require an extensive satellite survey. Understanding the factors that affect the surface albedo is also a complex problem, but a combination of statistical studies from a relatively high-resolution global satellite data set and careful surface/aircraft measurements may allow separation of the dominant factors.

c. *Snow cover*

The spectral dependence of snow reflectance makes the 0.6 μm wavelength measurements very sensitive to the presence of snow; however, the complex spatial patterns and time variations introduced by snow cover, especially on heterogeneous, vegetated surfaces, greatly complicates the analysis to remove clouds. (Our particular scheme made use of the IR spectral channel to separate snow-covered surfaces from clouds.) The success of the method illustrated here and by Rossow et al. (1987) supports the argument for a multispectral and statistical approach to these problems, but these results also need improvement. A tendency for increased average reflectance and increased brightening (snow-covered reflectance minus snow-free reflectance) is apparent in Table 3, apparently depending on vegetation density. However, the range of reflectance values exhibited by any snow-covered land type is very large. Although a "typical brightening" value can be defined from the results for several land-cover types, the large variation requires further study to identify its causes. With data covering more months and several years, stratified by time, viewing geometry, latitude and land type, we can attempt to separate factors associated with snow characteristics (such as depth and age) from vegetation characteristics (such as canopy structure and density). Monitoring snow effects in the near-IR will also be important to a proper specification of the snow-albedo feedback implied by different vegetation types.

d. *Future work*

The successes and failures of the analysis method used here, together with the statistical/diagnostical techniques employed to understand the results, suggest a strategy for improving measurements and understanding of processes which affect surface albedo. First, the differential sensitivity of various spectral channels, though not explicitly examined here, can be exploited to isolate clear scenes more reliably so that the statistics allow for examination of shorter time scale variations and angular dependence. Using data for the whole globe allows for study of systematic effects by intercomparison of similar targets, as well as determining the variability of various land types regionally and among continents. Multiyear satellite data sets allow for repeated comparisons of seasonal and snow effects to identify those that are controlled by surface properties, such as vegetation density. Given the limitations of currently available satellite radiometers, careful comparisons of satellite and ground-based observations will be necessary to convert these observations of spectral bidirectional reflectance into accurate surface *albedos* and an understanding of the factors controlling surface albedo for climate studies. Striving for such high accuracy is also necessary to allow for sensitive monitoring of surface albedo changes due to regional climate variations or human activities.

Acknowledgments. We would like to thank C. Brest and G. Seze for helpful discussions and suggestions during the course of this work. E. Kinsella, S. Chan and B. Suozzo provided valuable early assistance in handling the data. L. Del Valle and Mary Garcia are gratefully acknowledged for their patient and professional drafting and typing contributions.

REFERENCES

Allen, W. A., and A. J. Richardson, 1968: Interaction of light with a plant canopy. *J. Opt. Soc. Amer.*, **58**, 1023–1028.

Arnfield, A. J., 1975: A note on the diurnal, latitudinal and seasonal

variation of the surface reflection coefficient. *J. Appl. Meteor.*, **14**, 1603–1608.

Ashley, M. D., and J. Rea, 1975: Seasonal vegetation differences from ERTS imagery. *Photogram. Engin.*, **41**, 713–719.

Bauer, K. G., and J. A. Dutton, 1962: Albedo variations measured from an airplane over several types of surface. *J. Geophys. Res.*, **67**, 2367–2376.

Berglund, E. R., and A. C. Mace, Jr., 1972: Seasonal albedo variation of black spruce and sphagnum-sedge bog cover types. *J. Appl. Meteor.*, **11**, 806–812.

Billings, W. D., and R. J. Morris, 1951: Reflection of visible and infrared radiation from leaves of different ecological groups. *Amer. J. Bot.*, **38**, 237–331.

Brest, C., 1983: Seasonal variation and spatial distribution of surface reflectance and albedo: Satellite observations of an urban/rural landscape. Ph.D. Thesis (unpublished), Columbia University, 296 pp.

Brest, C. L., 1987: Seasonal albedo of an urban/rural landscape from satellite observations. *J. Climate Appl. Meteor.*, (in press).

——, and S. N. Goward, 1987: Deriving surface albedo measurements from narrow band satellite data. *Intl. J. Remote Sens.*, (in press).

Briegleb, B., and V. Ramanathan, 1982: Spectral and diurnal variations in clear sky planetary albedo. *J. Appl. Meteor.*, **21**, 1160–1171.

Briegleb, B. P., P. Minnis, V. Ramanathan and E. Harrison, 1986: Comparison of regional clear-sky albedos inferred from satellite observations and model computations. *J. Climate Appl. Meteor.*, **25**, 214–226.

Charney, J. C., 1975: Dynamics of deserts and drought in the Sahel. *Quart. J. Roy. Meteor. Soc.*, **101**, 193–202.

——, W. J. Quirk, S. H. Chow and J. Kornfield, 1977: A comparative study of the effects of albedo change on drought in semi-arid regions. *J. Atmos. Sci.*, **34**, 1366–1385.

Chen, T. S., and G. Ohring, 1984: On the relationship between clear-sky planetary and surface albedos. *J. Atmos. Sci.*, **41**, 156–158.

Chia, L.-S., 1967: Albedos of natural surfaces in Barbados. *Quart. J. Roy. Meteor. Soc.*, **93**, 116–120.

Condit, H. R., 1970: The spectral reflectance of American soils. *Photogram. Engin.*, **36**, 955–966.

Courel, M. F., R. S. Kandel and S. I. Rasool, 1984: Surface albedo and the Sahel Drought. *Nature*, **307**, 528–531.

Crane, R. G., and R. G. Barry, 1984: The influence of clouds on climate with a focus on high latitude interactions. *J. Climatol.*, **4**, 71–93.

Dickinson, R. E., 1983: Land surface processes and climate–surface albedos and energy balance. *Advances in Geophysics*, **25**, 305–354.

Duggin, M. J., 1985: Factors limiting the discrimination and quantification of terrestrial features using remotely sensed radiance. *Int. J. Remote Sens.*, **6**, 3–27.

Fuller, S. P., and W. R. Rouse, 1979: Spectral reflectance changes accompanying a postfire recovery sequence in a subarctic spruce lichen woodland. *Remote Sens. Environ.*, **8**, 11–23.

Gates, D. M., H. J. Keegan, J. C. Schleter and V. R. Weidner, 1965: Spectral properties of plants. *Appl. Opt.*, **4**, 11–20.

Gausman, H. W., 1977: Reflectance of leaf components. *Remote Sens. Environ.*, **6**, 1–9.

——, W. A. Allen, R. Cardenas and A. J. Richardson, 1970: Relation of light reflectance to histological and physical evaluations of cotton leaf maturity. *Appl. Opt.*, **9**, 545–552.

Grenfell, T. C., and G. A. Maykut, 1977: The optical properties of ice and snow in the Arctic Basin. *J. Glaciol.*, **18**, 445–463.

Gruber, A., and J. S. Winston, 1978: Earth-atmosphere radiative heating based on NOAA scanning radiometer measurements. *Bull. Amer. Meteor. Soc.*, **59**, 1570–1573.

Hansen, J., A. Lacis, D. Rind, G. Russell, P. Stone, I. Fung, R. Ruedy and J. Lerner, 1984: Climate sensitivity: Analysis of feedback mechanisms. *Climate Processes and Climate Sensitivity*. J. E. Hansen and T. Takahashi, Eds., *Geophys. Monogr. 29*, Amer. Geophys. Union, 130–163.

Herman, G., and R. Goody, 1976: Formation and persistence of summertime Arctic stratus clouds. *J. Atmos. Sci.*, **33**, 1537–1553.

Hilsenrath, E., and B. M. Schlesinger, 1981: Total ozone seasonal and interannual variations derived from the 7-year Nimbus-4 BUV data set. *J. Geophys. Res.*, **86**, 12087–12096.

Hoffman, G. R., 1970: Spectral properties of selected plant species and some variations accompanying leaf thickness, pigmentation and dehydration. *Proc. So. Dak. Acad. Sci.*, **49**, 60–72.

Howard, J. A., 1977: Aerial albedos of natural vegetation in south-eastern Australia. *Proc. Eleventh Int. Symp. on Rem. Sens. of Environ., Vol. 2*. Ann Arbor, 1301–1307.

Hummel, J. R., and R. A. Reck, 1979: A global surface albedo model. *J. Appl. Meteor.*, **18**, 239–253.

Jacobowitz, H., R. J. Tighe and the NIMBUS 7 ERB Experiment Team, 1984: The Earth Radiation Budget derived from the NIMBUS 7 ERB experiment. *J. Geophys. Res.*, **89**, 4997–5010.

Justice, C. O., J. R. G. Townshend, B. N. Holben and C. J. Tucker, 1985: Analysis of the phenology of global vegetation using meteorological satellite data. *Int. J. Remote Sens.*, **6**, 1271–1318.

Kanemasu, E. T., 1974: Seasonal canopy relectance patterns of wheat sorghum and soybean. *Remote Sens. Environ.*, **3**, 43–47.

Kimes, D. S., 1983: Dynamics of directional reflectance factor distributions for vegetation canopies. *Appl. Opt.*, **22**, 1364–1372.

——, 1984: Modeling the directional reflectance from complete homogeneous vegetation canopies with various leaf-orientation distributions. *Opt. Soc. Amer. A*, **1**, 725–737.

Knipling, E. B., 1970, Physical and physiological basis for the reflectance of visible and near-infrared radiation from vegetation. *Remote Sens. Environ.*, **1**, 155–159.

Kriebel, K. T., 1979: Albedo of vegetated surfaces: Its variability with differing irradiances. *Remote Sens. Environ.*, **8**, 283–290.

Kukla, G., and D. Robinson, 1980: Annual cycle of surface albedo. *Mon. Wea. Rev.*, **108**, 56–68.

Kung, E. C., R. A. Bryson and D. H. Lenschow, 1964: Study of a continental surface albedo on the basis of flight measurements and structure of the earth's surface cover over North America. *Mon. Wea. Rev.*, **92**, 543–564.

Lacis, A. A., and J. E. Hansen, 1974: A parameterization for the absorption of solar radiation in the earth's atmosphere. *J. Atmos. Sci.*, **31**, 118–133.

Leeman, V. 1972: The NASA Earth Resources Spectral Information System: A data compilation, first supplement. NASA CR-115757 [NTIS N72-30345].

——, D. Earing, R. Vincent and S. Ladd, 1971: The NASA Earth Resources Spectral Information System: A data compilation. NASA CR-115756 [NTIS N72-28366].

LeMaster, E. W., J. E. Chance and C. L. Wiegand, 1980: A seasonal verification of the Suits spectral reflectance model of wheat. *Photogram. Engin. Remote Sens.*, **46**, 107–114.

Markham, B. L., D. S. Kimes, C. J. Tucker and J. E. McMurtrey, 1981: Temporal spectral response of a corn canopy. *Photogram. Engin. Remote Sens.*, **11**, 1599–1605.

Matthews, E., 1983: Global vegetation and land use: New high-resolution data bases for climate studies. *J. Clim. Appl. Meteor.*, **22**, 474–487.

——, 1984: Prescription of land-surface boundary conditions in GISS GCM II: A simple method based on high-resolution vegetation data bases. NASA Tech. Memo. 86096, 20 pp.

——, 1985: Atlas of archived vegetation, land-use and seasonal albedo data bases. NASA Tech. Memo. 86199, 53 pp.

McFadden, J. D., and R. A. Ragotzkie, 1967: Climatological significance of albedo in central Canada, *J. Geophys. Res.*, **72**, 1135–1143.

Mekler, Y., and J. H. Joseph, 1983: Direct determination of surface albedos from satellite imagery. *J. Climate Appl. Meteor.*, **22**, 530–536.

Minnis, P., and E. F. Harrison, 1984: Diurnal variability of regional cloud and clear-sky radiative parameters derived from GOES data. Part I: Analysis method. *J. Climate Appl. Meteor.*, **23**, 993–1011.

Monteith, J. L., 1975: *Vegetation and the Atmosphere, Vol. 1, Principles.* Academic, 278 pp.

——, 1976: *Vegetation and the Atmosphere, Vol. 2, Case Studies.* Academic, 436 pp.

——, and G. Szceicz, 1961: The radiation balance of bare soil and vegetation. *Quart. J. Roy. Meteor. Soc.,* **87,** 159–170.

Norton, C. C., F. R. Mosher and B. Hinton, 1979: An investigation of surface albedo variations during the recent Sahel drought. *J. Appl. Meteor.,* **18,** 1352–1362.

Oguntoyinbo, J. S., 1970: Reflection coefficient of natural vegetation, crops and urban surfaces in Nigeria. *Quart. J. Roy. Meteor. Soc.,* **96,** 430–441.

Olson, C. E., Jr., and R. E. Good, 1962: Seasonal changes in light reflectance from forest vegetation. *Photogram. Engin.,* **28,** 107–114.

Oxford World Atlas, 1973: S. G. Cohen, Ed., Oxford Univ. Press, 190 pp.

Petzold, D. E., and A. N. Rencz, 1975: The albedo of selected subarctic surfaces. *Arc. and Alp. Res.,* **7,** 393–398.

Pinty, B., and G. Szejwach, 1985: A new technique for inferring surface albedo from satellite observations. *J. Climate Appl. Meteor.,* **24,** 741–750.

Posey, J. W., and P. F. Clapp, 1964: Global distribution of normal surface albedo. *Geofis. Int.,* **4,** 33–48.

Preuss, H. J., and J. F. Geleyn, 1980: Surface albedos derived from satellite data and their impact on forecast models. *Arch. Meteor. Geophys. Bioklim., Ser. A.,* **29,** 345–356.

Raschke, E., and H. J. Preuss, 1979: The determination of the solar radiation budget at the earth's surface from satellite measurements. *Meteor. Rdsch.,* **32,** 18–28.

——, T. H. Vonder Haar, W. R. Bandeen and M. Pasternak, 1973: The annual radiation balance of the earth–atmosphere system during 1969–70 from Nimbus 3 measurements. *J. Atmos. Sci.,* **30,** 341–364.

Richardson, A. J., and H. W. Gausman, 1982: Reflectance differences between untreated and mepiquat chloride-treated, field-grown cotton through the growing season. *Remote Sens. Environ.,* **12,** 501–507.

Robinson, D. 1984: Anthropogenic impact on winter surface albedo. Ph.D. thesis (unpublished), Columbia University.

Robinson, D. A., and G. Kukla, 1985: Maximum surface albedo of seasonally snow-covered lands in the Northern Hemisphere. *J. Climate Appl. Meteor.,* **24,** 402–411.

Robock, A., 1980: The seasonal cycle of snow cover, sea ice and surface albedo. *Mon. Wea. Rev.,* **108,** 267–285.

——, and D. Kaiser, 1985: Satellite-observed reflectance of snow and clouds. *Mon. Wea. Rev.,* **113,** 2023–2029.

Rockwood, A. A., and S. K. Cox, 1976: Satellite inferred surface albedo over northwestern Africa. *Atmos. Sci. Paper 265,* Dept. of Atmos. Sci., Colorado State University, 64 pp.

Root, R. R., and L. D. Miller, 1971: Identification of urban watershed units using remote multispectral sensing. Environmental Resources Center Completion Rep. OWRR Project No. A-012-COLO, Colorado State University, 51 pp + 6 appendices.

Rossow, W. B., L. C. Garder, E. Kinsella, A. A. Lacis and C. L. Brest, 1987: Global and seasonal cloud variations from satellite radiance, measurements: 1. Analysis method. *J. Climate Appl. Meteor.,* to be submitted.

Sato, M., K. Kawabata and J. E. Hansen, 1977: A fast invariant imbedding method for multiple scattering calculations and an application to equivalent widths of CO_2 lines on Venus. *Astrophys. J.,* **216,** 947–962.

Scott, D., P. H. Menalda and R. W. Brougham, 1968: Spectral analysis of radiation transmitted and reflected by different vegetations. *N. Z. J. Bot.,* **6,** 427–449.

Stanhill, G., G. J. Hofstede and J. D. Kalma, 1966: Radiation balance of natural and agricultural vegetation. *Quart. J. Roy. Meteor. Soc.,* **92,** 128–140.

Staylor, W. F., and J. T. Shuttles, 1986: Reflection and emission models for deserts derived from Nimbus-7 ERB scanner measurements. *J. Climate Appl. Meteor.,* **25,** 196–202.

Sud, Y. C., and M. J. Fennessy, 1982: A study of the influence of surface albedo on July circulation in semiarid regions using the GLAS GCM. *J. Climatol.,* **2,** 105–125.

Swain, P. H., and S. M. Davis, 1978: Remote Sensing: The Quantitative Approach. McGraw-Hill, 289 pp.

Taylor, V. R., and L. L. Stowe, 1984: Reflectance characteristics of uniform earth and cloud surfaces derived from NIMBUS-7 ERB, *J. Geophys. Res.,* **89,** 4987–4996.

Toon, O. B., and J. B. Pollack, 1976: A global average model of atmospheric aerosols for radiative transfer calculations. *J. Appl. Meteor.,* **15,** 225–246.

Tucker, C. J., 1978: Post senescent grass canopy remote sensing. *Remote Sens. Environ.,* **7,** 203–210.

——, J. R. G. Townshend and T. E. Goff, 1985: African land-cover classification using satellite data. *Science,* **227,** 369–375.

——, B. N. Holben, J. H. Elgin and J. E. McMurtrey, 1981: Remote sensing of total dry-matter accumulation in winter wheat. *Remote Sens. Environ.,* **11,** 171–189.

——, ——, —— and ——, 1980: Relationship of spectral data to grain yield variation. *Photogram. Engin. Remote Sens.,* **46,** 657–666.

Vonder Haar, T. H., and V. E. Suomi, 1971: Measurements of the earth's radiation budget from satellites during a five-year period. Part I: Extended time and space means. *J. Atmos. Sci.,* **28,** 305–314.

Vulis, I., A. Lacis, W. B. Rossow and D. Vulis, 1987: Radiative modeling and information content analysis of multichannel AVHRR satellite measurements. *J. Geophys. Res.,* to be submitted.

Warren, S. G., 1982: Optical properties of snow. *Rev. Geophys. Space Phys.,* **20,** 67–89.

Wetherald, R. T., and S. Manabe, 1975: The effects of changing the solar constant on the climate of a general circulation model. *J. Atmos. Sci.,* **32,** 2044–2058.

Wilson, M. F., 1984: Construction and use of surface information in a general circulation climate model. Unpublished Ph.D. thesis, University of Liverpool.

Wiscombe, W. J., and S. G. Warren, 1981: A model for the spectral albedo of snow. I: Pure snow. *J. Atmos. Sci.,* **37,** 2712–2745.

Woolley, J. T., 1971: Reflectance and transmittance of light by leaves. *Plant Physiol.,* **47,** 656–662.